Justus- Liebig- Universität Gießen
II. Physikalisches Institut

Master Thesis

Simulation of X(3872) Decays Using the PandaRoot Framework

Simulation von X(3872)-Zerfällen mit dem PandaRoot Framework

written by

Martin Johannes Galuska*

May 2011

Supervisors: Prof. Dr. Wolfgang Kühn
AR Dr. Jens Sören Lange

*Martin.J.Galuska@physik.uni-giessen.de

Abstract

The $\overline{\mathsf{P}}$ANDA experiment – which will be built as part of the planned FAIR expansion of the existing GSI facility – will offer internal dense targets and cooled antiproton beams provided by the storage ring HESR.

The X(3872) is a resonance which has been seen in several decay channels by numerous experiments around the world. Currently, for its width, only an upper limit of 2.3 MeV at 90% confidence level is published [1].

In this work a detailed simulation of a resonance scan of the X(3872) with the $\overline{\mathsf{P}}$ANDA experiment is performed within the PandaRoot framework. 20 equidistant energy scan points of two days of data taking each with an accelerator duty factor of 50% and HESR in high resolution mode are assumed. The beam energy distribution is approximated by a Gaussian.

For the signal reconstruction, the X(3872) decay channel into $J/\psi\ \pi^+\pi^-$ is chosen and a cross section of $\sigma[\mathrm{p\overline{p}} \to \mathrm{X}(3872) \to J/\psi\ \pi^+\pi^-] = 5$ nb is assumed. The X(3872) cross section is parametrized by a Breit-Wigner distribution with a constant X(3872) width of 100 keV. The J/ψ is reconstructed from its decay into $\mathrm{e^+e^-}$. A compilation of the assumed parameters for the simulation is given in table 4 in appendix A.

Final state radiation is simulated, initial state radiation is assumed to play a minor part. A constant background with a cross section of 1.2 nb [2] from the process $\mathrm{p\overline{p}} \to J/\psi\ \pi^+\pi^-$ is taken into account for the resonance scan. Inelastic hadronic background from a dual parton model based generator is studied using two different sets of two million events each. For the resonance scan simulation these processes are assumed to be rejectable for the considered reconstruction channel by combining the electron/pion discrimination implemented in this work with cuts on missing and invariant mass. However, larger Monte Carlo samples using more computing power will be necessary to determine the effect of the inelastic hadronic background. The software implemented in this work is designed to be used for highly automated and parallelized processing and will be applied to produce and analyse large amounts of simulated background events.

On the aforementioned assumptions the simulation shows that a resonance scan of X(3872) might be feasible with the $\overline{\mathsf{P}}$ANDA experiment. From the simulated experimental data, the reconstructable X(3872) width $\Gamma_{\mathrm{X}(3872)}$ is estimated using the approximation $\Gamma_{\mathrm{X}(3872)} \simeq W_{\mathrm{obs}} - \frac{(1.02 \cdot W_{\mathrm{G}})^2}{W_{\mathrm{obs}}}$ which introduces a systematic error of less than 4% [3]. The full width at half maximum W_{obs} of the observed excitation function's line shape is estimated by a fit of a convolution of Gaussian and Breit-Wigner. The FWHM W_{G} of a Gaussian distribution parametrizing the measurement errors is assumed to be dominated by the center of mass energy spread which arises from the limited beam momentum resolution of $\Delta p_{\mathrm{beam}}/p_{\mathrm{beam}} \leq 2 \cdot 10^{-5}$ for HESR in high resolution mode. The outlined method yields an estimate on $\Gamma_{\mathrm{X}(3872)}$ of 110.0 keV which is 10% larger than the input width. The error of this estimate should be dominated by the estimation of W_{G} and the statistical fluctuations of the observed signal counts and not by using the above approximation.

Zusammenfassung

Das $\overline{\text{P}}$ANDA Experiment, welches als Teil der geplanten FAIR Erweiterung der bestehenden GSI-Anlage errichtet werden soll, bietet interne Targets mit hoher Dichte und phasenraumgekühlte Antiprotonenstrahlen, die vom Speicherring HESR bereitgestellt werden.

Das X(3872) ist eine Resonanz, die in mehreren Zerfallskanälen von zahlreichen Experimenten auf der ganzen Welt gesehen wurde. Derzeit ist für dessen Breite $\Gamma_{\text{X(3872)}}$ lediglich eine obere Grenze von $2,3$ MeV bei einem Konfidenzniveau von 90% veröffentlicht worden [1].

In dieser Arbeit wird eine detaillierte Simulation eines Resonanzscans des X(3872) mit dem $\overline{\text{P}}$ANDA Experiment im PandaRoot Framework durchgeführt. Es werden 20 äquidistante Energiescanpunkte simuliert, die jeweils zwei Tagen Datenaufnahme bei einer Beschleunigerauslastung von 50% entsprechen. Für HESR wird der hochauflösende Betriebsmodus gewählt. Die Verteilung der Schwerpunktsenergie wird durch eine Gaußverteilung angenähert.

Für die Signal- Rekonstruktion wird der X(3872) Zerfallskanal nach $J/\psi\ \pi^+\pi^-$ gewählt und es wird von einem Wirkungsquerschnitt von $\sigma[\text{p}\overline{\text{p}} \to \text{X(3872)} \to J/\psi\ \pi^+\pi^-] = 5$ nb ausgegangen, welcher durch eine Breit-Wigner-Verteilung mit konstanter X(3872) Breite von 100 keV parametrisiert wird. Das J/ψ wird durch seinen Zerfall in e^+e^- rekonstruiert. Tabelle 4 in Anhang A enthält eine Zusammenstellung der angenommenen Parameter für die Simulation.

Final State Radiation ist in der Simulation berücksichtigt, während angenommen wird, dass Initial State Radiation eine untergeordnete Rolle spielt. Die Simulation des Resonanzscans berücksichtigt einen konstanten $\text{p}\overline{\text{p}} \to J/\psi\ \pi^+\pi^-$ Untergrund mit einem abgeschätzten Wirkungsquerschnitt von 1,2 nb [2].

Untergrund aus inelastischen hadronischen Reaktionen wird separat anhand von zwei verschiedenen simulierten Datensätzen mit je zwei Millionen Ereignissen untersucht, die mit einem auf dem Dual Parton-Modell basierenden Ereignisgenerator erzeugt werden. Für die Simulation des Resonanzscans wird angenommen, dass dieser Untergrund in dem betrachteten Rekonstruktionskanal durch die Kombination von Schnitten sowohl auf fehlende als auch auf invariante Masse mit der Elektronen-/ Pionen Diskriminierung, die in dieser Arbeit entwickelt und implementiert wurde, unterdrückt werden kann.

Allerdings ist die Simulation einer größeren Menge von Monte Carlo Daten mit mehr Rechenleistung erforderlich, um den Effekt des inelastischen hadronischen Untergrunds abschließend klären zu können. Die Software, die in dieser Arbeit entwickelt wurde, eignet sich zur automatisierten und hochgradig parallelisierten Erzeugung und Analyse großer Mengen von simulierten Untergrund Ereignissen und wird zukünftig auch für diesen Zweck verwendet werden.

Die unter den oben genannten Annahmen durchgeführte Simulation zeigt, dass ein realer Resonanzscan des X(3872) mit dem $\overline{\text{P}}$ANDA Experiment durchführbar sein könnte. Die aus den simulierten Daten rekonstruierbare X(3872) Breite $\Gamma_{\text{X(3872)}}$ wird mit Hilfe der Näherung

$\Gamma_{\mathrm{X(3872)}} \simeq W_{\mathrm{obs}} - \frac{(1{,}02 \cdot W_{\mathrm{G}})^2}{W_{\mathrm{obs}}}$ abgeschätzt, welche einen systematischen Fehler von weniger als 4% [3] mit sich bringt. Die volle Halbwertsbreite W_{obs} der gemessenen Linienform der Anregungsfunktion wird durch einen Fit mit einer Faltung von Gauß- und Breit-Wigner-Verteilung abgeschätzt. Für die volle Halbwertsbreite W_{G} einer Gauß-Verteilung, die die Messfehler parametrisiert, wird angenommen, dass sie durch die Schwerpunktsenergieverteilung dominiert wird. Diese ergibt sich aus der begrenzten Strahlimpulsauflösung von $\Delta p_{\mathrm{beam}}/p_{\mathrm{beam}} \leq 2 \cdot 10^{-5}$ für den hochauflösenden HESR Betriebsmodus. Die skizzierte Abschätzung liefert einen Näherungswert für $\Gamma_{\mathrm{X(3872)}}$ von 110,0 keV, und somit einen 10% größeren Wert als die gewählte echte Breite von genau 100 keV. Der Fehler dieses Ergebnisses sollte hauptsächlich durch die Abschätzung von W_{G} und die statistischen Schwankungen der beobachteten Signale bestimmt sein. Der systematische Fehler der verwendeten Näherungsformel sollte einen vergleichsweise geringen Einfluss auf das erhaltene Ergebnis haben.

Contents

List of Figures

List of Tables

1. Motivation

1.1. The Standard Model

The Standard Model of Physics describes how all known matter is built up and how it interacts.

Particles: In general, particles can be classified by their *spin* which is a fundamental characteristic of the particle's quantum state. Particles of integer[1] spin are called *bosons*. Identical bosons can occupy the same quantum state and play an important role as force carrier particles. Particles that have half integer spins are called *fermions*. They respect the *Pauli exclusion principle* which states that two identical fermions cannot be simultaneously in the same quantum state. Fermions can be further divided into *quarks* and *leptons*. This distinction becomes evident in the paragraphs on the weak and the strong interactions. The Standard Model requires only six quarks and six leptons to explain how all known matter is built up, and to every fermion there exists a corresponding antiparticle which carries opposite charges.

Interactions: The Standard Model describes three fundamental interactions by the means of *Quantum Field Theory*[2]. To each interaction there are characteristic *Force Carrier Particles* of spin $J = 1$. The term "gauge boson" is used interchangeably with "force carrier". Not every force acts on every Standard Model particle. The gauge bosons couple to certain kinds of charge which are characteristic for the interaction and therefore only affect particles that carry a nonzero quantity of such a charge.

The photon is the force carrier particle of the electromagnetic interaction which was created by unifying the electric and the magnetic interaction with the Maxwell equations. It couples to electric charge and therefore, neutral particles do not interact electromagnetically.

The weak interaction acts on all leptons with the same strength. This is referred to as *universality*. However, the coupling strength to quarks appears to be non-universal. In order to preserve universality, Cabibbo introduced weak eigenstates. These are obtained from mass eigenstates by a rotation with an angle which is called *Cabibbo angle*. Cabibbo originally only accounted for the two quark generations which were known at that time. The CKM (Cabibbo-Kobayashi-Maskawa) matrix is the generalization for three generations. The squared absolute values of its entries represent the probabilities that a given quark changes its flavor and becomes a quark with a difference in electric charge of $\pm 1e$ by emitting or absorbing a W^+ or a W^- boson. Glashow, Illiopoulos and Maiani were able to explain why neutral flavor changing currents are strongly suppressed [4]. Therefore, quarks do not change their flavor when they absorb or emit the electrically neutral Z^0. The weak interaction is the only force that violates parity symmetry P: Its three gauge bosons couple only to the left-handed

[1] In particle physics it is customary to choose units in which Planck's constant h divided by 2π (also denoted by $\hbar$) is equal to 1. Additionally, all speeds are measured as fractions of the speed of light c which as a consequence is equal to 1 as well. These units are used throughout this thesis.

[2] A short introduction can be found in [5].

component of particles and the right-handed component of antiparticles. Therefore, it is said to be *maximally parity violating*. CP-violation has also been observed and whether the CPT symmetry holds is still an open question and a field of active research.[3] Its short range is due to the high masses of its force carrier particles, the $W^{\pm}$ and the Z^0.

Salam and Weinberg were able to unify the weak and the electromagnetic interactions creating the theory of the *electroweak interaction*, but due to *spontaneous symmetry breaking* the weak interaction behaves significantly different than the electromagnetic interaction. Therefore, both interactions are usually regarded as two individual forces – similar to treating liquids and gases as distinct states of matter.

The strong interaction is mediated by gluons which couple to a strong color charge. Only quarks, antiquarks and gluons themselves carry this kind of charge. Therefore, gluons can couple to other gluons. This leads to the effect of a running coupling constant α_S (see figure 1): At short distances, quarks behave like no forces acted upon them. This effect is called *asymptotic freedom*. However, when one tries to separate two quarks, there is a force between them which is believed to remain constant as their distance is increased. The gluon string field between the two quarks accumulates enough energy for a new quark-antiquark pair to be created from the vacuum. This process leads to a *confinement* of quarks which means that neither quarks nor antiquarks can exist as free particles. They are always bound to hadrons which can be categorized into *baryons* consisting of three constituent quarks or antiquarks and *mesons* which are strong interaction bound states of one quark and one antiquark. The quantum field theory describing the strong interaction is called *quantum chromodynamics* and is usually abbreviated as *QCD*. Its corresponding charge is called *color* due to its analogies to the additive color mixing in TV screens. The color charge has three manifestations: Red, green and blue. Quarks carry color, antiquarks carry anticolor and every hadron has to be in a color neutral state[4] at all times. Gluons carry both color and anticolor at the same time.

Gravitation is the only interaction known so far which is not contained within the Standard Model. Even though its effects are negligible for particle physics' processes in which only a few fundamental particles interact, the fact that the Standard Model is lacking a quantum field theory describing gravitation means that the Standard Model is not complete. There exist numerous possible theories for *Physics Beyond the Standard Model*[5] and a considerable number of experiments has been searching for experimental indications for new physics.

Table 1 lists the fundamental building blocks and some of their properties. Notice the organization into *three families* containing four particles each – a neutral lepton, a charged lepton, a negatively charged quark, and a positively charged quark. As indicated in the table, the main distinction between leptons and quarks is that quarks can interact strongly while leptons cannot. Interestingly, all known stable matter is built up from the two quarks of the first

[3] C stands for charge conjugation symmetry and T denotes the symmetry under time inversion. If the CP-symmetry was not violated, physical processes would be the same if all particles were interchanged with their according antiparticles and in addition space was inverted – which is aquivalent to swapping left and right. CPT symmetry adds time inversion which corresponds to a reversion of all momenta.

[4] Color cancels out its corresponding anticolor to form a color neutral state. All three forms of color added together are colorless. The same is true for a combination of all three anticolors.

[5] For further information see for instance chapter 12 of [5].

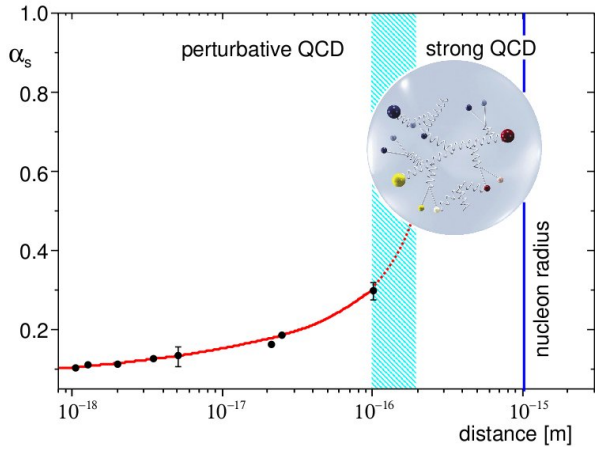

Figure 1: Illustration of the coupling constant α_s of the strong interaction as a function of the distance in meter as shown in [6]. For quark distances comparable to the size of a nucleon the gluon field accumulates enough energy to create quark-antiquark pairs. This property of the strong interaction is called confinement. The data points represent experimental values from [7].

family and the electron. Protons, for instance, consist of two up-quarks and one down-quark; neutrons are comprised of one up-quark and two down-quarks.

The question why there are exactly three families of fundamental particles is still unanswered. However, the possibility that there might be additional, so far undiscovered families is rather small. The width of the Z^0-resonance is the strongest indication for this fact, because it proves that there are only three neutrinos with masses smaller than the mass of the Z^0-particle. Since all three known neutrinos have a rather small mass[6], it is somewhat unlikely that there is a fourth very massive one.

Fermions	Families			Electric Charge [e]	Strong Charge	Weak Charge
	1	2	3			
Quarks	**u**p	**c**harm	**t**op	+2/3	✔	✔
	down	**s**trange	**b**ottom	−1/3	✔	✔
Leptons	ν_e	ν_μ	ν_τ	0	✗	✔
	e	μ	τ	-1	✗	✔

Table 1: The fundamental fermions of the Standard Model and some of their properties. The usual abbreviations of quark names are set in boldface.
The electric charges are measured in multiples of the electron charge $e = 1.602 \cdot 10^{-19}$ C.

Table 2 lists the Force Carriers of the Standard Model. The theoretically proposed *Higgs-Boson* is not listed, because it has not been discovered to date. The *Higgs-formalism* [5] is a

[6]Ever since neutrino-oscillations have been discovered it is known that the masses of neutrinos cannot be equal to zero. The exact masses have not been measured yet, only upper limits are known so far (see [1]).

possible explanation of how fundamental particles get their masses. It is based on spontaneous symmetry breaking by a scalar field, which hides the aforementioned electroweak symmetry. If there is such a field, it should be possible to measure its excitation in form of a particle which is called the Higgs-Boson. The limits for its mass[7] are more than about 100 GeV (experimentally) and less than about 1,000 GeV (theoretically). It is hoped that the issue of the existence of the Higgs-Boson can be clarified with the *LHC (Large Hadron Collider)*.

Interaction	Force Carrier	Coupling to	Mass [GeV]	Charge	
Electromagnetic	γ	Electric Charge	$< 1 \cdot 10^{-27}$	None	
Weak	$W^{\pm}$ Z^0	Flavor	80.399 ± 0.023 91.1876 ± 0.0021	$\pm 1\ e$ $0\ e$	Weak Charge
Strong	g	Color Charge	0	Color *and* Anti-Color	

Table 2: Overview of the experimentally observed Standard Model interactions' force carriers. All masses are taken from [1] as of April 2011. The mass of the gluon g is a theoretical value. A small mass of a couple of MeV would not be in contradiction with the experiments.
As the table shows, gluons, $W^{\pm}$- and Z^0-bosons carry the kind of charge that they couple to. This property allows for so-called self-coupling.

While the Standard Model is a well tested theory, there are numerous questions left unanswered. How do the fundamental Standard Model particles get their masses? Can all known interactions be unified? Why are there exactly three families? Why is there more matter than antimatter in the universe? It is expected that answers to some of these questions can be found at the TeV scale, i.e. with the currently running CERN (European Organization for Nuclear Research) experiments.

However, even if the process of how fundamental building blocks get their masses was well known, the Standard Model would still be far from being able to explain why the proton has a mass of 938.272013 ± 0.000023 MeV [1] as less than 10% of this number is due to the masses of the proton's constituent quarks.

[7] In particle physics energies are usually measured in the unit of electron-Volts (eV). 1 eV is the kinetic energy that one unbound electron gains when it is accelerated by a voltage of 1 V. For particles at rest, the energy mass relation $E = mc^2$ holds and allows to measure masses in units of energies when the speed of light c is set to 1.

1.2. Heavy Quarkonium Spectroscopy

As pointed out in section 1.1, it is well-known that the Standard Model is not "the last word". The theoretical and experimental search for theories beyond it is driven by questions such as: Why do coupling constants and particle masses have the values which are experimentally measured? Can the Standard Model parameters such as particle masses and CKM mixing angles be derived from first principals? A complementary approach to the aforementioned experiments at the TeV scale is *heavy quarkonium spectroscopy*. It can be used to probe all regimes of QCD from low energies in which non-perturbative effects are dominant to high energies in which perturbation theory can be applied. Most notably, it is a well suited tool to test the energy regime in between those two extremes.

The term *quarkonium* designates mesons that are built up of a quark and its corresponding antiquark. Such mesons are called *flavorless*, because quarks and antiquarks carry opposite signs of the additive flavor quantum number. Heavy quarkonium refers to *charmonium* in which a c quark is bound to a $\bar{c}$ antiquark and *bottomonium* which are $b\bar{b}$ bound states. For light pseudo-scalar ($J^{PC} = 0^{-+}$) quark-antiquark states $u\bar{u}$, $d\bar{d}$ and $s\bar{s}$ quantum mechanical mixing of the states can be experimentally observed, because the masses of the up, down and strange quarks are quite similar. The much larger mass differences between the bottom and charm quarks and the three lighter quarks result in states that are well defined in terms of the quark-antiquark pair flavor. A $t\bar{t}$ bound state (*toponium*) cannot be formed, because the very massive top quark decays too rapidly via the electroweak interaction.

Different quarkonium states which consist of the same kind of quark-antiquark pairs are usually distinguished by their quantum numbers: The *spin* J of quarkonium can be calculated by coupling the spins of its constituent quark-antiquark pair to obtain S and vector adding the orbital angular momentum of the quark-antiquark pair L. For quarkonium the *parity* quantum number P is related to the orbital angular momentum via the equation $P = (-1)^{L+1}$ and its *charge conjugation* quantum number[8] is connected to the coupled quark spins and the orbital angular momentum via $C = (-1)^{L+S}$. P and C are multiplicative quantum numbers while spins and angular momenta are vector additive.

Two kinds of notations are used to classify quarkonium states: The quantum numbers can be written according to the scheme[9] J^{PC}. The second possibility is the so-called spectroscopic notation: $n^{2S+1}L_J$ with n being the principal quantum number which is calculated via $n = N+1$ from the number of zeroes N of the radial wave function. The orbital angular momentum L is usually represented by a capital letter which symbolizes its value according to the following scheme: $L = 0\widehat{=}$S, $L = 1\widehat{=}$P, $L = 2\widehat{=}$D, $L = 3\widehat{=}$F and so on. The third possibility is to use Greek letters to denote quarkonium states. The spin 1 charmonium ground state J/ψ is an exception due to historic reasons. However, the "J" is dropped in the notation for its excited states such as the ψ'.

In general, QCD allows the calculation of meson properties from its constituents, but perturbation theory cannot be used to calculate decay rates and static properties such as masses

[8] A charge conjugation quantum number C is defined for neutral particles only.
[9] For non-neutral particles, the notation is reduced to J^P.

and widths. The only general method is lattice QCD computation, the other option is to use models. For light quarks the motion is highly relativistic in mesons, because mesons are in general much heavier than their constituent quarks. Relativistic effects are expected to be less dominant in charmonium and bottomonium as the c and b quarks are much more massive. Therefore, the computation can be approximated by an expansion in powers of the estimated quark speed v which is about 0.1 for bottomonium and 0.3 for charmonium. This technique is called non-relativistic QCD.

Another popular approach that allows for accurate predictions of quarkonia parameters without lengthy lattice QCD calculations is to assume that the quarks move in a static effective potential such as the so-called Cornell potential

$$V(r) = -\frac{4}{3} \cdot \frac{\alpha_S(r)}{r} + k \cdot r \tag{1}$$

with r being the effective quarkonium radius. The typical region of interest corresponds to $0.1 \text{ fm} \leq r \leq 1.0 \text{ fm}$. The potential in (1) has a Coulomb-like part for one-gluon exchanges between the quark and its antiquark which is dominant at short distances r and a confinement part which parameterizes the non-perturbative effects of QCD and dominates for large r. Additional effects can be incorporated by introducing more terms to the potential such as (compare to [8]):

Spin-orbit term	$+\frac{1}{2m^2}\left(\frac{4\alpha_S(r)}{r^3} - \frac{k}{r}\right)\vec{L}\cdot\vec{S}$
Tensor term	$+\frac{4}{3}\frac{\alpha_S(r)}{m^2}\frac{1}{r^3}\left(3(\vec{S_1}\cdot\hat{r})(\vec{S_2}\cdot\hat{r}) - \vec{S_1}\cdot\vec{S_2}\right)$
Spin-spin interaction potential	$+\frac{32\pi}{9}\frac{\alpha_S(r)}{m^2}\vec{S_1}\cdot\vec{S_2}\delta(r)$

In case of charmonium, m denotes the mass of the c quark and for bottomonium it stands for the b quark mass. $\vec{S_1}$ and $\vec{S_2}$ denote the spins of the quark and the antiquark, respectively. $\delta(r)$ is the Dirac δ-distribution and $\hat{r}$ is the relative position vector of the quark-antiquark pair. $\vec{L}$ is their orbital angular momentum. $\vec{S} = \vec{S_1} + \vec{S_2}$ is the spin of the meson. Note that in the above ansatz the confinement potential contributes to the spin-orbit term.

In this method, a potential such as the one given in equation (1) with additional terms and wave functions for the quark- antiquark system are assumed. The radial wavefunction equation (2) which is obtained from the stationary two-body Schrödinger equation is solved

numerically[10]. The calculated results are fitted to the masses of well-measured quarkonium states in order to determine the parameters α_S and k.

$$\left[-\frac{1}{m}\left(\frac{d^2}{dr^2}+\frac{2}{r}\frac{d}{dr}+\frac{l(l+1)}{r^2}\right)+V(r)+2m\right]R_n(r)=E_nR_n(r) \tag{2}$$

$R_n(r)$ is the radial wave function of the quark-antiquark system and E_n is the energy of the system in the according eigenstate. The angular momentum quantum number is denoted by $l \in \mathbb{N}_0$.

By determining which bound states of a heavy quark and its corresponding antiquark exist and measuring their masses, widths and quantum numbers, nonperturbative QCD can be put to the test. It also allows to find evidence for new physics at moderate energies. One of the most intriguing questions that could be answered with heavy quarkonium spectroscopy is whether exotic states such as quark-gluon hybrids and tetraquarks exist or if such states have already been observed. A very interesting resonance with a mass in the charmonium region is the so-called X(3872) which is discussed in section 1.3.

[10]See [9] and references therein.

1.3. The X(3872) Resonance

The X(3872) is a resonance that was first discovered by Belle in $B^{\pm} \to K^{\pm}$ X(3872) $\to K^{\pm}\ J/\psi\ \pi^+\pi^-$ decays [10]. Since then, the decay channel X(3872) $\to J/\psi\ \pi^+\pi^-$ has been confirmed by numerous experiments [11, 12, 13], most recently by the LHCb collaboration [14]. Several additional decay channels [1] were found such as:

- X(3872) $\to J/\psi\ \gamma$
- X(3872) $\to D^0\bar{D}^{*0}$
- X(3872) $\to D^0\bar{D}^0\pi^0$

The observed decay into $J/\psi\ \gamma$ allows the assignment of positive charge conjugation $C = +1$. This is supported by the fact that the narrow peak seen in the discovery channel is possibly absent in the invariant mass spectrum of the final state $J/\psi\ \pi^+\pi^-$ in e^+e^- collisions [1]. A high statistics analysis by CDF [15] allows two quantum number assignments: $J^{PC} = 1^{++}$ and $J^{PC} = 2^{-+}$. A paper by Belle favors 1^{++} [16] while BaBar favors 2^{-+} [17]. The resonance scan simulation carried out in this thesis assumes that the 1^{++} assignment holds.

Several experiments around the world have seen the X(3872) in numerous decay channels. Therefore, it is safe to say that the X(3872) is a well-established resonance with a mass $m_{\mathrm{X(3872)}} = 3871.56 \pm 0.22$ MeV [1] in the charmonium realm, but its structure is still unclear. As pointed out in [2] many interpretations exist. It was suggested that the X(3872) could be the first excited state of conventional charmonium $\chi_{c1}(2P)$ [18]. Other models consider it to be an S-wave threshold effect of $D^0\bar{D}^{*0}$ [19] or attempt to explain it as a cusp effect [20], a diquark anti-diquark bound state [21], a hybrid charmonium [22] or even a tetraquark state [23]. The possibility that the X(3872) might be a $D^0\bar{D}^{*0}$ molecule [24] is appealing, because its mass is rather close to the sum of the masses of D^0 and $\bar{D}^{*0}$. If accurate measurements showed that the X(3872) mass was actually greater than the sum of the masses of D^0 and $\bar{D}^{*0}$ this would disprove the possibility that it could be a molecule of those two particles with positive binding energy. However, a virtual $D^0\bar{D}^{*0}$ state with negative binding energy would still be possible.

To date, little information is available about the X(3872) resonance. For its width $\Gamma_{\mathrm{X(3872)}}$ there is only an upper limit of 2.3 MeV [1] at 90% confidence level published. The actual value could be significantly smaller.

Its cross section for formation in $p\bar{p}$ annihilations with a subsequent decay into the $J/\psi\ \pi^+\pi^-$ channel is estimated in [2] using model based calculations for the $D^0\bar{D}^{*0}$ molecule interpretation and for the $\chi_{c1}(2P)$ possibility. The authors publish that $\sigma[p\bar{p} \to \mathrm{X(3872)} \to J/\psi\ \pi^+\pi^-]$ should be within the interval from 3.57 to 443 nb for the assumption that the X(3872) is a loosely bound molecule of $D^0\bar{D}^{*0}$. Assuming the X(3872) is $\chi_{c1}(2P)$ the calculated range is 2.19 to 238 nb. The results strongly depend on $\Gamma_{\mathrm{X(3872)}}$ as a parameter which the authors consider to be between 136 keV and 2.3 MeV. The dependence of the estimated total cross

sections at threshold is illustrated in figure 2. Smaller widths yield larger estimated cross sections.

A resonance scan (see section 4.3) is a suitable experimental method for high precision measurements. It could be applied to measure $\Gamma_{\mathrm{X}(3872)}$ in order to advance the to date quite limited knowledge about the X(3872). As explained in section 4.2, a direct X(3872) production in e^+e^- is prohibited due to the positive charge conjugation rendering $p\overline{p}$ annihilations to be ideal for an accurate investigation of the X(3872) lineshape. The $\overline{\mathsf{P}}\mathsf{ANDA}$ experiment which is discussed in section 4.1 will combine superb PID capabilities with cooled antiproton beams of unprecedented momentum resolution provided by its antiproton storage ring HESR (see section 4.2). These unique possibilities will allow $\overline{\mathsf{P}}\mathsf{ANDA}$ to contribute to the determination of the nature of this mysterious resonance X(3872).

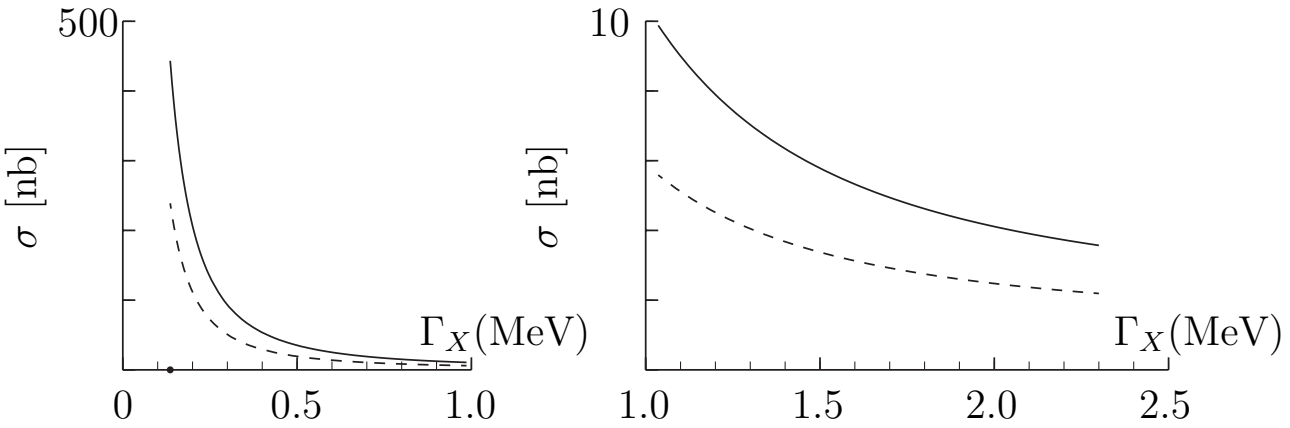

Figure 2: The estimated total cross section $\sigma[p\overline{p} \to \mathrm{X}(3872) \to J/\psi\, \pi^+\pi^-]$ at the threshold as a function of the X(3872) width $\Gamma_{\mathrm{X}(3872)}$ as published in [2]. The solid and dashed lines represent the interpretation of X(3872) as a molecule of D-mesons and as $\chi_{c1}(2P)$, respectively.

2. Objective of this Work

In section 1.3 it was noted that the width of the X(3872) is currently unknown. To date only an upper limit for $\Gamma_{X(3872)}$ of 2.3 MeV at 90% confidence level is published [1]. A resonance scan (see section 4.3) is a well suited method to improve the knowledge about this fundamental parameter.

The main goal of this work is to simulate a resonance scan with a cooled antiproton beam at the $\overline{\mathsf{P}}$ANDA experiment under realistic assumptions[11]. The entire simulation chain and the analysis are conducted in the PandaRoot framework (see section 4.4) for an input width $\Gamma_{X(3872)} = 100$ keV and an assumed cross section[12] $\sigma[p\overline{p} \to X(3872)] = 50$ nb. All detectors that are currently implemented in the framework are taken into account as well as detailed magnetic field maps. Track finder and track fitter algorithms are used for pattern recognition to achieve a realistic signal reconstruction. Final state radiation is taken into account using the PHOTOS package (see section 6). For the cross section of the X(3872) a Breit-Wigner distribution is considered. The beam momenta are assumed as Gaussians and the effects on the line shape of the resonance's excitation curve is investigated.

In addition, a detailed simulation of hadronic background reactions from a dual parton model (DPM) generator (see section 5.3) in the center of mass energy region corresponding to the mass of the X(3872) is carried out.

Furthermore, an electron/pion discrimination using the matching of charged particle tracks reconstructed from MVD and TPC measurements and clusters measured in the EMC is implemented.

As the PandaRoot framework is continously being improved and there exist multiple possible detector layouts for $\overline{\mathsf{P}}$ANDA, the development of a software base for further resonance scan simulations has a high priority in this work. With every major update of the framework or change in the detector setup the detailed results of a simulated resonance scan might slightly differ. Therefore, a high level of automatization and reusability of the tools developed in this work is pursued. Furthermore, an adaption for related or more detailed studies is intended to be easy.

An additional goal pursued in the software development for this work is to take advantage of today's and future multi-core computer systems and so-called *batch farms* which have become very common in scientific milieus. The tools written for this thesis are to be used with *Torque Maui*[13], but can easily be adapted for other batch software.

[11] A discussion of the simulation parameters can be found in section 5.1.

[12] Cross sections are usually measured in the unit barn which is abbreviated by b and 1 b $= 10^{-28}$ m^2.

[13] Torque Maui refers to a software combination of the TORQUE (Terascale Open-Source Resource and QUEue Manager) Resource Manager [25] and the *Maui Cluster Scheduler* [26]. Both programs are widely-used open source software. Torque Maui is also deployed on our workgroup's computing cluster which is described in appendix D. All plots and results presented in this work were obtained from simulations carried out on the aforementioned cluster.

3. Mathematical Methods

3.1. Invariant Mass

A common problem in particle physics is to reconstruct the mass of a particle R from its decay products. Assuming that particle R decays into n particles B_i with $i \in \{1, \ldots, n\}, n \in \mathbb{N}_+$,

$$R \to B_1 \; B_2 \; \ldots \; B_n \tag{3}$$

a formula to calculate the invariant mass can be derived from the relativistic energy-momentum relation which is given by

$$E^2 = \vec{p}^2 + m^2. \tag{4}$$

E denotes the energy of a given particle, $\vec{p}$ is its three dimensional momentum vector and m is its mass. The according *four dimensional momentum vector* is written as $(E, \vec{p})^T$ and usually called *four-vector* or *four-momentum* for short. The absolute value of such a vector is Lorentz-invariant and therefore equal to the mass m of the particle. It can be calculated according to the following equation which is a reformulation of (4):

$$m = \left|(E, \vec{p})^T\right| = \sqrt{E^2 - \vec{p}^2}. \tag{5}$$

Energy-momentum-conservation implies that the four-vector of R has to be equal to the sum of the four-vectors of all decay products B_i. Therefore, adding all those four-momenta and then calculating the Lorentz invariant absolute value of the resulting four vector according to equation (5) gives the result shown in equation (6) which is called *invariant mass*:

$$m_{\text{inv}} = \sqrt{\left(\sum_{i=1}^{n} E_{B_i}\right)^2 - \left(\sum_{i=1}^{n} \vec{p}_{B_i}\right)^2}. \tag{6}$$

It is important to note that all energies and momenta in equation (6) have to be measured with respect to the same frame of reference. If the energies E_{B_i} and momenta $\vec{p}_{B_i}$ of all decay products are measured with zero error, the calculated value m_{inv} is equal to the mass m_R. Of course, this is not true if any of the particles B_i did not originate from the decay of particle R.

3.2. Missing Mass

Consider a process in which the total center of mass energy E_{cm} is converted into a single resonance R which subsequently decays into n particles B_i with $i \in \{1, \ldots, n\}, n \in \mathbb{N}_+$:

$$R \to B_1 \; B_2 \; \ldots \; B_j \; \ldots \; B_n. \tag{7}$$

The according four-momenta in the center of mass frame of reference are $\left(E_{\text{cm}}, \vec{0}\right)^T$ for the resonance R and $(E_{B_i}, p_{\vec{B_i}})^T$ for its decay products.

Assuming all decay particles but one (B_j with $j \in \{1, \ldots, n\}$) can be reconstructed, the mass m_{B_j} of the missing decay product can be calculated using the energy-momentum-relation (4) and the conservation of four-momenta in particle decays:

$$\left(E_{\text{cm}}, \vec{0}\right)^T = \sum_{i=1}^{n} (E_{B_i}, p_{\vec{B_i}})^T = \left(E_{B_j}, p_{\vec{B_j}}\right)^T + \sum_{\substack{i=1 \\ i \neq j}}^{n} (E_{B_i}, p_{\vec{B_i}})^T . \tag{8}$$

Subtracting the sum on the right hand side on both sides of equation (8) gives

$$\left(E_{\text{cm}} - \sum_{\substack{i=1 \\ i \neq j}}^{n} E_{B_i}, \vec{0} - \sum_{\substack{i=1 \\ i \neq j}}^{n} p_{\vec{B_i}} \right)^T = \left(E_{B_j}, p_{\vec{B_j}}\right)^T . \tag{9}$$

Calculating the abolute values of the four-vectors in equation (9) results with a formula for the mass of B_j:

$$m_{B_j} = \sqrt{\left(E_{\text{cm}} - \sum_{i \neq j} E_{B_i} \right)^2 - \sum_{i \neq j} \vec{p}^{\,2}_{B_i}}. \tag{10}$$

For any set of $n-1$ particles that do not necessarily come from the same decay this formula can be generalized to

$$m_{\text{missing}} = \sqrt{\left(E_{\text{cm}} - \sum_{i \neq j} E_{B_i} \right)^2 - \sum_{i \neq j} \vec{p}^{\,2}_{B_i}}. \tag{11}$$

m_{missing} is equal to m_{B_j} if all energies and momenta in equation (11) were measured with zero error and if all the particles in the set really come from the same decay. It is important to note that all decay particle energies and momenta in equation (11) have to be measured in the center of mass frame of reference of resonance R.

Equation (11) is also very helpful if the properties of all decay particles are measured. It can be used to help reduce background from particle misidentification. If it is experimentally hard to determine which particles originate from which event, it can also be successfully deployed.

3.3. Gaussian Distribution

The Gaussian function

$$f(x) = \frac{1}{\sqrt{2\pi}\cdot\sigma}\cdot\exp\left(-\frac{(x-x_0)^2}{2\sigma^2}\right) \tag{12}$$

is the probability density function of the *normal distribution* – which is also called *Gaussian distribution* – with mean $x_0 \in \mathbb{R}$ and *standard deviation* $\sigma > 0$.

The maximum point of f is x_0. Due to the axial symmetry of f about $x = x_0$ there exist two half-maximum points x_1 and x_2 which can be found by solving the following equation:

$$\begin{aligned}
f(x_{1/2}) &= \frac{1}{2}\cdot f(x_0) \\
\frac{1}{\sqrt{2\pi}\cdot\sigma}\cdot\exp\left(-\frac{(x_{1/2}-x_0)^2}{2\sigma^2}\right) &= \frac{1}{2}\cdot\frac{1}{\sqrt{2\pi}\cdot\sigma}\cdot\underbrace{\exp\left(-\frac{(x_0-x_0)^2}{2\sigma^2}\right)}_{=1} \\
\exp\left(-\frac{(x_{1/2}-x_0)^2}{2\sigma^2}\right) &= \frac{1}{2} \\
-\frac{(x_{1/2}-x_0)^2}{2\sigma^2} &= \ln\left(\frac{1}{2}\right) = -\ln(2) \\
(x_{1/2}-x_0)^2 &= 2\sigma^2\ln(2) \\
x_{1/2} &= x_0 \pm \sqrt{2\ln(2)}\cdot\sigma
\end{aligned}$$

The *full width at half maximum (FWHM)* is the relative distance of the half-maximum points x_1 and x_2 which is now easy to calculate:

$$|x_1 - x_2| = 2\cdot\sqrt{2\ln(2)}\cdot\sigma = \sqrt{8\ln(2)}\cdot\sigma.$$

The relation between the full width at half maximum of a Gaussian and its standard deviation is therefore given by

$$\mathrm{FWHM}(\sigma) = \sqrt{8\ln(2)}\cdot\sigma \simeq 2.3548200\cdot\sigma. \tag{13}$$

3.4. Error Propagation

The standard deviation Δf of a function f which depends on n uncorrelated Gaussian distributed parameters $x_i,\ i \in \{1,\ldots,n\}$ with standard deviations denoted by Δx_i can approximatively be calculated according to the error propagation given in equation (14):

$$\Delta f(x_1,\ldots,x_n) = \sqrt{\sum_{i=1}^{n}\left(\frac{\partial f}{\partial x_i}\cdot\Delta x_i\right)^2}. \tag{14}$$

3.5. Resonance Formation in $p\overline{p}$-Annihilations

Resonant cross sections are generally described by the Breit-Wigner formula. The spin-averaged Breit-Wigner cross section $\sigma_{\mathrm{BW}}(E_{\mathrm{cm}})$ for the formation and subsequent decay of an isolated spin-J resonance R with mass M_R and small[14] total full width Γ_R at half maximum in the collision of two particles (other than photons) of spin S_1 and S_2 respectively, is given by

$$\sigma_{\mathrm{BW}}(E_{\mathrm{cm}}) = \frac{(2J+1)}{(2S_1+1)\cdot(2S_2+1)} \cdot \frac{\pi}{k^2} \cdot \frac{B_{\mathrm{in}} \cdot B_{\mathrm{out}} \cdot \Gamma_R^2}{(E_{\mathrm{cm}} - E_R)^2 + \Gamma_R^2/4} \tag{15}$$

(compare to [1]). B_{in} and B_{out} are the branching fractions of the resonance R into the entrance and exit channels. E_R is its rest energy. E_{cm} is the center of mass energy and k is the center of mass momentum in the initial state.

For a fixed target experiment in which a moving particle with mass m_1 collides with a resting particle of mass m_2, k^2 can be calculated from the squared laboratory momentum ${p_{\mathrm{beam}}}^2$ of the moving particle and the center of mass energy E_{cm} via equation

$$k^2 = {p_{\mathrm{beam}}}^2 \cdot \frac{m_2^2}{{E_{\mathrm{cm}}}^2} \tag{16}$$

which can also be found in [1].

In case an antiproton $\overline{\mathrm{p}}$ beam is shot onto a proton p target, the according Lorentz vectors are given by $p_{\overline{\mathrm{p}}} = \left(\sqrt{m_{\mathrm{p}}^2 + {p_{\mathrm{beam}}}^2}, 0, 0, p_{\mathrm{beam}}\right)^T$ and $p_{\mathrm{p}} = (m_{\mathrm{p}}, 0, 0, 0)^T$. m_{p} denotes the mass of one proton or antiproton. ${E_{\mathrm{cm}}}^2$ is easily obtained by calculating the Lorentz invariant square of the sum of the aforementioned 4-vectors which is $p_{\overline{\mathrm{p}}}+p_{\mathrm{p}} = \left(\sqrt{m_{\mathrm{p}}^2 + {p_{\mathrm{beam}}}^2} + m_{\mathrm{p}}, 0, 0, p_{\mathrm{beam}}\right)^T$:

$$\begin{aligned} {E_{\mathrm{cm}}}^2 &= \left(m_{\mathrm{p}}^2 + {p_{\mathrm{beam}}}^2\right) + m_{\mathrm{p}}^2 + 2m_{\mathrm{p}} \cdot \sqrt{m_{\mathrm{p}}^2 + {p_{\mathrm{beam}}}^2} - {p_{\mathrm{beam}}}^2 \\ &= 2m_{\mathrm{p}}^2 + 2m_{\mathrm{p}} \cdot \sqrt{m_{\mathrm{p}}^2 + {p_{\mathrm{beam}}}^2}. \end{aligned} \tag{17}$$

Solving equation (17) for ${p_{\mathrm{beam}}}^2$ gives

$$\begin{aligned} {p_{\mathrm{beam}}}^2 &= \left(\frac{{E_{\mathrm{cm}}}^2 - 2m_{\mathrm{p}}^2}{2m_{\mathrm{p}}}\right)^2 - m_{\mathrm{p}}^2 \\ &= \frac{{E_{\mathrm{cm}}}^4 - 4m_{\mathrm{p}}^2 \cdot {E_{\mathrm{cm}}}^2 + 4m_{\mathrm{p}}^4}{4m_{\mathrm{p}}^2} - \frac{4m_{\mathrm{p}}^2}{4m_{\mathrm{p}}^2} \cdot m_{\mathrm{p}}^2 \\ &= {E_{\mathrm{cm}}}^2 \cdot \frac{{E_{\mathrm{cm}}}^2 - 4m_{\mathrm{p}}^2}{4m_{\mathrm{p}}^2} \end{aligned} \tag{18}$$

[14] If the width Γ_R is not small, it cannot be treated as being constant in equation (15). In the Monte Carlo simulation the decaying resonance is X(3872) with a width $\Gamma_{\mathrm{X(3872)}}$ that is chosen to be equal to 100 keV. This allows to treat $\Gamma_{\mathrm{X(3872)}}$ as a constant in the above formula.

which can be plugged into equation (16) to give

$$\begin{aligned} k^2 &= \left({E_{\mathrm{cm}}}^2 \cdot \frac{{E_{\mathrm{cm}}}^2 - 4m_{\mathrm{p}}^2}{4m_{\mathrm{p}}^2} \right) \cdot \frac{m_{\mathrm{p}}^2}{{E_{\mathrm{cm}}}^2} \\ &= \frac{{E_{\mathrm{cm}}}^2 - 4m_{\mathrm{p}}^2}{4}. \end{aligned} \tag{19}$$

Using this result for k^2 and plugging in the known spins $S_1 = S_2 = \frac{1}{2}$ for the proton and the antiproton, equation (15) is reduced to

$$\begin{aligned} \sigma_{\mathrm{BW}}(E_{\mathrm{cm}}) &= \frac{(2J+1)}{4} \cdot \frac{4\pi}{{E_{\mathrm{cm}}}^2 - 4m_{\mathrm{p}}^2} \cdot \frac{\mathrm{BR}(R \to \mathrm{p\overline{p}}) \cdot \mathrm{BR}(R \to f) \cdot \Gamma_R^2}{(E_{\mathrm{cm}} - E_R)^2 + \Gamma_R^2/4} \\ &= \frac{(2J+1) \cdot 4\pi}{{E_{\mathrm{cm}}}^2 - 4m_{\mathrm{p}}^2} \cdot \frac{\mathrm{BR}(R \to \mathrm{p\overline{p}}) \cdot \mathrm{BR}(R \to f) \cdot \Gamma_R^2}{4(E_{\mathrm{cm}} - E_R)^2 + \Gamma_R^2} \end{aligned} \tag{20}$$

in which f denotes the final state of interest. $\mathrm{BR}(R \to \mathrm{p\overline{p}})$ and $\mathrm{BR}(R \to f)$ denote the branching ratios for the resonance into the entrance and exit channels.

In analogy to equation (2.5) in [27] the expected number of formations and subsequent decays $n(E_{\mathrm{cm0}})$ for the process $\mathrm{p\overline{p}} \to R \to f$ can be calculated by multiplying the Breit-Wigner cross section $\sigma_{\mathrm{BW}}(E_{\mathrm{cm}})$ given in equation (20) with the center of mass energy distribution $B(E_{\mathrm{cm}}, E_{\mathrm{cm0}})$ of the utilized machine for a given nominal center of mass energy E_{cm0}, integrating over the energy acceptance of the detector and multiplying the result with the integrated luminosity $\mathcal{L}_{\mathrm{int}}$:

$$n(E_{\mathrm{cm0}}) = \mathcal{L}_{\mathrm{int}} \cdot \int \sigma_{\mathrm{BW}}(E_{\mathrm{cm}}) \cdot B(E_{\mathrm{cm}}, E_{\mathrm{cm0}})\, dE_{\mathrm{cm}} \tag{21}$$

The expected value for the observed number of signals is obtained by multiplying $n(E_{\mathrm{cm0}})$ with the detector efficiency for the observed final state f and the nominal center of mass energy E_{cm0}.

Equation (21) can be reformulated in terms of an effective cross section $\sigma_{\mathrm{eff}}(E_{\mathrm{cm0}})$

$$n(E_{\mathrm{cm0}}) = \mathcal{L}_{\mathrm{int}} \cdot \sigma_{\mathrm{eff}}(E_{\mathrm{cm0}}) \tag{22}$$

by simply defining the integral in equation (21) as an effective cross section:

$$\sigma_{\mathrm{eff}}(E_{\mathrm{cm0}}) = \int \sigma_{\mathrm{BW}}(E_{\mathrm{cm}}) \cdot B(E_{\mathrm{cm}}, E_{\mathrm{cm0}})\, dE_{\mathrm{cm}}. \tag{23}$$

Figuratively speaking: The shape of the Breit-Wigner cross section is distorted by the center of mass energy distribution which is accounted for by introducing the effective cross section.

As in section 2.4.4 of [27] the simplified, but reasonable, assumption is made that the center of mass energy E_{cm} is Gaussian distributed (see section 3.3) about its nominal value E_{cm0} with

standard deviation $\Delta E_{\mathrm{cm}0}$ which itself depends on $E_{\mathrm{cm}0}$ (see section 4.2 for a calculation of the standard deviation for a given nominal center of mass energy):

$$B(E_{\mathrm{cm}}, E_{\mathrm{cm}0}) = \frac{1}{\sqrt{2\pi} \cdot \Delta E_{\mathrm{cm}0}} \cdot \exp\left(-\frac{(E_{\mathrm{cm}} - E_{\mathrm{cm}0})^2}{2(\Delta E_{\mathrm{cm}0})^2}\right) \tag{24}$$

From equations (21) and (23) the interpretation of the Breit-Wigner cross section $\sigma_{\mathrm{BW}}(E_{\mathrm{cm}})$ in equation (20) becomes evident: $\sigma_{\mathrm{BW}}(E_{\mathrm{cm}})$ is the cross section for the process $\mathrm{p\overline{p}} \to R \to f$ for a monoenergetic center of mass energy E_{cm} that is exactly equal to $E_{\mathrm{cm}0}$ and therefore, $B(E_{\mathrm{cm}}, E_{\mathrm{cm}0})$ can be represented by a Dirac δ-distribution $B(E_{\mathrm{cm}}, E_{\mathrm{cm}0}) = \delta(E_{\mathrm{cm}} - E_{\mathrm{cm}0})$:

$$\sigma_{\mathrm{eff}}(E_{\mathrm{cm}0}) = \int \sigma_{\mathrm{BW}}(E_{\mathrm{cm}}) \cdot \delta(E_{\mathrm{cm}} - E_{\mathrm{cm}0})\, dE_{\mathrm{cm}} = \sigma_{\mathrm{BW}}(E_{\mathrm{cm}0})$$

If all masses and energies are plugged into equation (20) in GeV, then the result is given in $\frac{1}{\mathrm{GeV}^2}$ and can be transformed into nanobarn (nb) with the conversion constant $1 = (\hbar c)^2 = 389379.304$ nb GeV^2.

4. Experimental Methods

4.1. The $\overline{\text{P}}$ANDA Detector

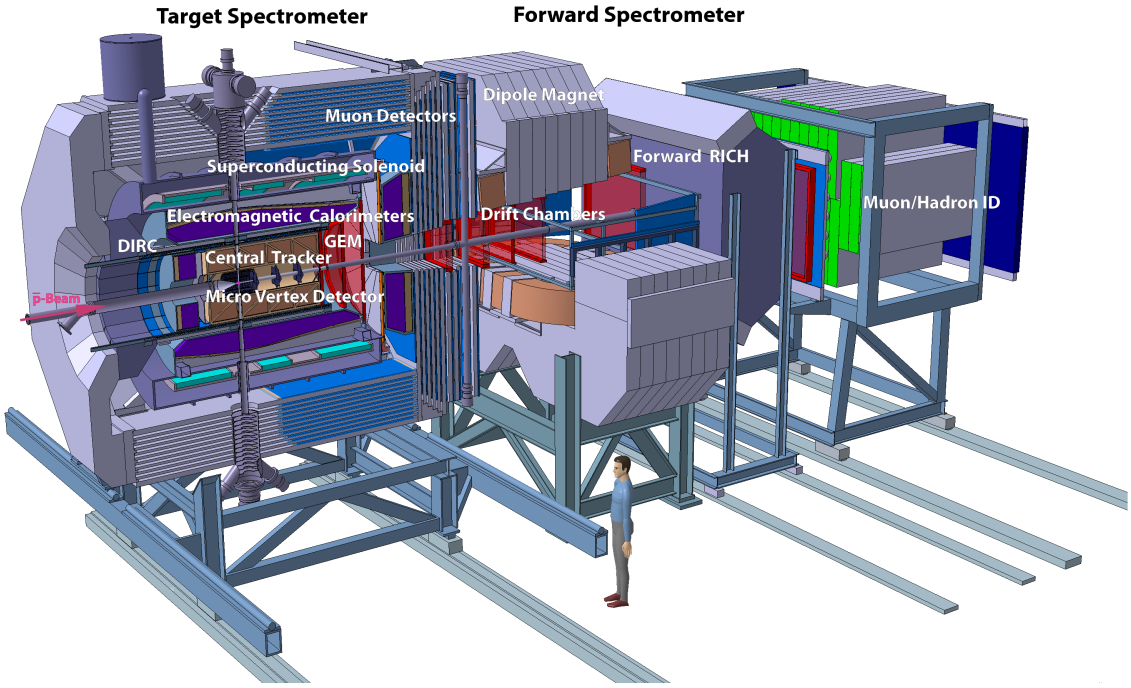

Figure 3: Artistic view of the $\overline{\text{P}}$ANDA Detector as shown in [27]. The target spectrometer with electronics and supplies is designed to be mounted on rails.

The $\overline{\text{P}}$ANDA (Anti-Proton Annihilations at Darmstadt) experiment is designed to investigate $\text{p}\overline{\text{p}}$ and $\overline{p}$+A collisions with an internal proton (p) or nuclear (A) target and an anti-proton beam in the momentum range from about 1 to 15 GeV which corresponds to a center of mass energy between about 2.0 and 5.5 GeV. It is part of the future FAIR (Facility for Anti-Proton and Ion Research, see fig. 4) extension of the existing GSI (Heavy Ion Research Lab) facility in Darmstadt, Germany.

The requirements for the $\overline{\text{P}}$ANDA experiment are quite high: The detector was designed to achieve nearly 4π solid angle coverage with good particle identification capabilities and high resolutions for particle tracking and calorimetry. Its readout needs to be capable of handling high rates up to $2 \cdot 10^7$ interactions per second and the event selection should be as versatile as possible.

The $\overline{\text{P}}$ANDA experiment combines a phase-space cooled antiproton beam with dense internal targets to offer unique possibilities for studies of numerous aspects of the strong interaction. Three different target types are foreseen:

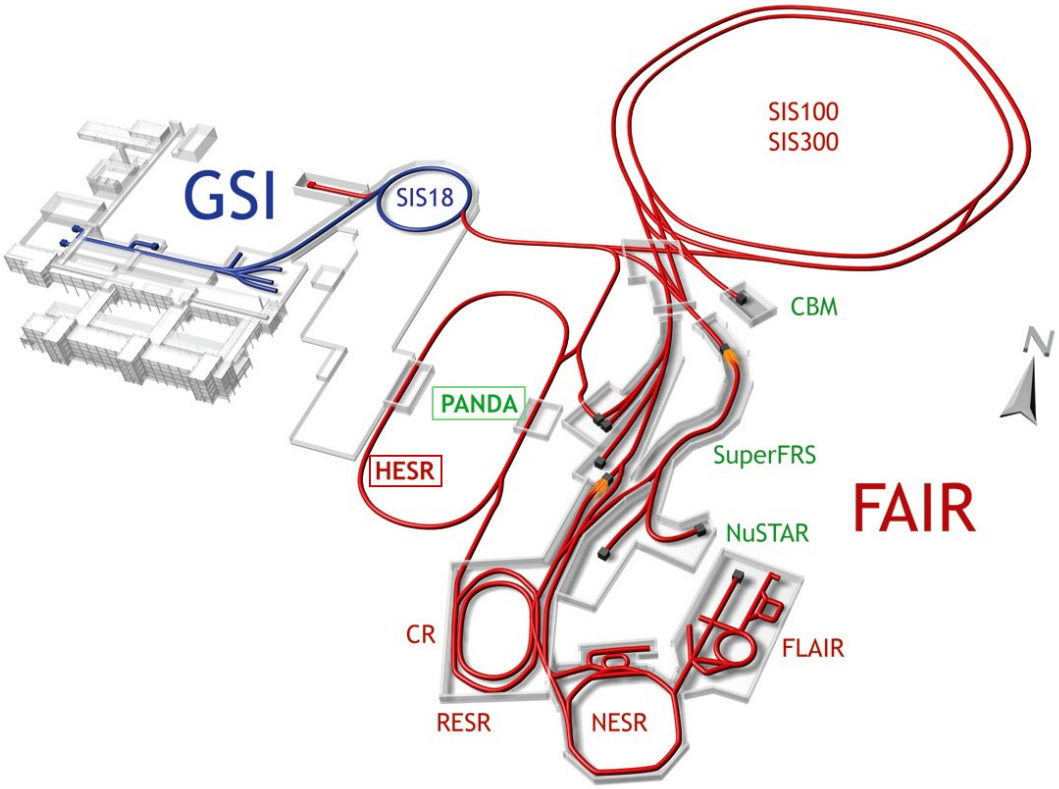

Figure 4: Layout of the existing GSI facility (in blue) and the planned FAIR expansion (in red) as published in [6]. Indicated are the locations of various planned experiments, synchrotrons as well as storage, accumulator and collector rings. The $\overline{\text{P}}$ANDA experiment and the HESR are highlighted. More details can be found in [28].

Pellet target Hydrogen pellets which are frozen hydrogen micro-spheres will traverse the antiproton beam perpendicularly with velocities of about 60 m/s. The pellet target can also be used with heavier gases.

Cluster jet target Pressurized cold gas is expanded into vacuum through a special nozzle which leads to condensation forming a narrow jet. This target technology can be used for hydrogen and heavier gases.

Fixed nuclear targets The detector's modular build allows for other types of targets such as Be, C, Si or Al to be inserted.

Utilizing a hydrogen target $\overline{\text{P}}$ANDA can access charmonium resonances R of all non-exotic quantum numbers in direct formation $\text{p}\overline{\text{p}} \rightarrow R$ whereas e^+e^- collisions are limited to formation of $J^{PC} = 1^{--}$ resonances due to the intermediate photon.

In order to optimize the momentum resolution the detector is split into two spectrometer parts (see figure 3). In each part charged particle identification, tracking and electromagnetic

calorimetry are available "to allow to detect the complete spectrum of final states relevant for the $\overline{\text{P}}$ANDA physics objectives." [27]

The target spectrometer surrounds the interaction point and therefore, is used to measure particles at high polar angles ϑ to the z-axis which points into the direction of the incident antiproton beam. Its onion-shell-like layout with a *barrel* and an *endcap* part is typical for modern particle physics experiments, but as $\overline{\text{P}}$ANDA is a fixed target experiment, most particles to be measured will go into the forward region and therefore, the design is asymmetric.

The innermost layer of the barrel is a *silicon vertex detector* which surrounds the interaction point and is mainly used to measure secondary vertices. For this reason it is usually referred to as *microvertex detector (MVD)*. Its additional purpose is to improve transverse momentum resolution of charged particles which are measured by the surrounding *central tracker*. Either a *straw tube tracker (STT)* or a *time-projection chamber (TPC)* will be utilized as central tracker. Both are required to allow for adequate momentum resolution $\delta p/p$ on the percent level and they have to be capable of handling high particle fluxes. This is especially challenging for the TPC. An additional intended use of the central tracker is to detect secondary vertices which can occur outside the MVD. The forward angles will be covered with three *Gas Electron Multiplier (GEM) planes* that are placed downstream of the target. *Cherenkov detectors* and a *time-of-flight system* are foreseen to be used in order to provide charged particle identification of hadrons and leptons over a large range of angles and momenta. The particle identification will be enhanced by the detection of internally reflected Cherenkov light with both *barrel and forward endcap DIRC detectors*.

The *electromagnetic calorimeter (EMC)* utilizes lead tungstate ($PbWO_4$) crystals which allow for very fast photon detection down to a few MeV with sufficient energy resolution. To increase the light yield the crystals will be cooled down to $-25°C$ both in the barrel and forward end-cap. For its cooled $PbWO_4$ EMC crystals the $\overline{\text{P}}$ANDA collaboration pioneered the technology of *stimulated recovery*. It allows for online healing of crystal structure damages which arise due to irradiation.

The 2 T magnetic field is provided by a *superconducting solenoid*. To minimize the amount of material in front of the EMC, the solenoid is placed around it. *Muon detectors* are implemented in its return yoke. In order to keep the cost for the solenoid and the crystal calorimeter to a minimum, the target spectrometer was designed to be very compact as a comparison with a person in figure 3 shows. As illustrated, the pipes for the injection of target material will cross the target spectrometer at an right angle to the beam pipe.

The modular design of the target spectrometer allows for removing the backward endcap calorimeter to add a dedicated nuclear target station and additional detectors for γ spectroscopy which is required for hypernuclei study.

The forward spectrometer is located downstream of the interaction region and measures particle tracks at small polar angles ϑ. Its magnetic field with a maximum bending power of 2 Tm is provided by a dipole magnet and covers the entire angular acceptance of the forward spectrometer.

In order to track high-momentum particles as well as particles with very low momenta (which curl up inside the magnetic field) two sets of wire chambers will be placed in front, within and behind the dipole magnet. For particle identification purposes in the forward region, a *ring imaging Cherenkov (RICH) detector*, a *time-of-flight wall*, a *Shashlyk-type forward electromagnetic calorimeter* and *forward muon detectors* are foreseen.

The HESR beam pipe goes through the center of the forward spectrometer which allows to reuse the beam for target interaction in the following revolutions.

The $\overline{\mathsf{P}}$ANDA experiment will offer superb PID capabilities. It will use a cooled antiproton beam which allows for unprecedented center of mass energy resolutions. This is a perfect combination for resonance scans (see section 4.3) in which the center of mass energy is determined by the known nominal antiproton momentum and the detector is only used for counting. The aforementioned cooled antiproton beam will be provided by the High Energy Storage Ring HESR which is the topic of the section 4.2.

4.2. The High Energy Storage Ring (HESR)

The $\overline{\text{P}}$ANDA detector offers unique opportunities for high precision measurements which are only possible in combination with a state of the art storage ring such as the planned HESR (High Energy Storage Ring). It is designed to use electron and stochastic cooling systems [29, 30] and features two operation modes: A high-luminosity mode with up to 10^{11} antiprotons in the beam, and a high-resolution mode with a design relative momentum spread $\Delta p_{\text{beam}}/p_{\text{beam}}$ of less than or equal to $2{\cdot}10^{-5}$. Fig. 5 shows HESR's racetrack-like shape: Two arc sections are connected by two long straight sections which host the electron cooler as well as the stochastic cooling pickup (P) and kicker (K).

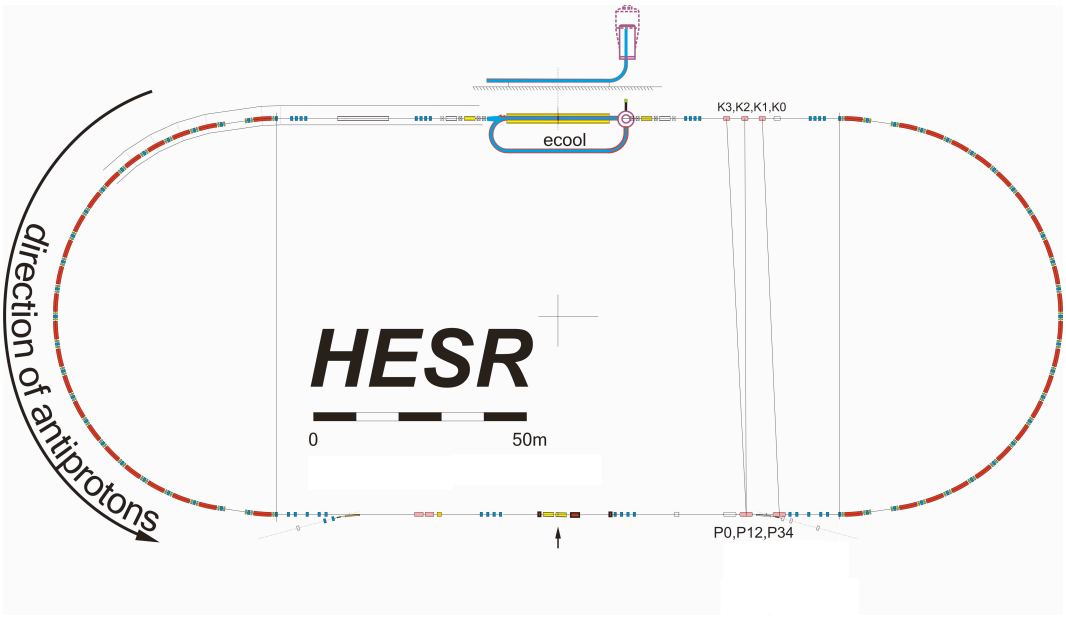

Figure 5: Schematic view of the HESR with tentative positions for injection, cooling devices and experimental installations as indicated in [27]. The $\overline{\text{P}}$ANDA detector will be located at the straight section opposite of the electron cooling system labeled as "ecool". The target area is indicated with an arrow.

For the antiproton production a proton beam with energies in the range from 30 to 90 GeV and an intensity up to $2 \cdot 10^{13}$ particles per second will be provided by the primary synchrotrons SIS-100 and SIS-300. The antiprotons are produced by a secondary target and then stored and cooled in the HESR.

Running HESR in the high resolution mode at center of mass energy E_{cm} adjusted to the mass $m_{\text{X(3872)}} \simeq 3.872$ GeV of the X(3872) corresponds to a nominal beam momentum $p_{\text{beam}} \simeq 6.988$ GeV (see equation 18). The antiproton momenta are assumed to be Gaussian distributed around this value with a standard deviation

$$\Delta p_{\text{beam}} = \underbrace{p_{\text{beam}}}_{\simeq 6.988\ \text{GeV}} \cdot \underbrace{\Delta p_{\text{beam}}/p_{\text{beam}}}_{=2{\cdot}10^{-5}\ \text{(see table 3)}} \simeq 139.76\ \text{keV}. \tag{25}$$

Experimental Requirements	
Ion species	Antiprotons $\overline{\mathrm{p}}$
$\overline{\mathrm{p}}$ production rate	$2 \cdot 10^7$ s^{-1} ($1.2 \cdot 10^{10}$ per 10 min)
Momentum / Kinetic energy range	1.5 to 15 GeV / 0.83 to 14.1 GeV
Number of particles	10^{10} to 10^{11}
Operation Modes	
High resolution (HR)	Luminosity $\mathcal{L}$ of $2 \cdot 10^{31}$ cm^{-2} s^{-1} for 10^{10} $\overline{\mathrm{p}}$ rms momentum spread $\Delta p_{\mathrm{beam}}/p_{\mathrm{beam}} \leq 2 \cdot 10^{-5}$ p_{beam} range from 1.5 to 9 GeV electron cooling up to $p_{\mathrm{beam}} = 9$ GeV
High luminosity (HL)	Luminosity $\mathcal{L}$ of $2 \cdot 10^{32}$ cm^{-2} s^{-1} for 10^{11} $\overline{\mathrm{p}}$ rms momentum spread $\Delta p_{\mathrm{beam}}/p_{\mathrm{beam}} \sim 10^{-4}$ p_{beam} range from 1.5 to 15 GeV stochastic cooling for $p_{\mathrm{beam}} > 3.8$ GeV

Table 3: Adapted excerpt from table 2.1 in [27] showing the key experimental requirements and the two operation modes for the HESR.

It is important to note that p_{beam} is much larger than the mass of the proton m_{p}. Therefore, an approximatively Gaussian p_{beam} distribution leads to a center of mass energy distribution that can be approximated by a Gaussian[15], as well. Its standard deviation can be calculated according to the propagation of uncertainty given in equation (14). The result is dominated by the beam momentum spread. The small standard deviation of the proton mass m_{p} measurement (see section 1.1) can be neglected. This leads to the following expression:

$$
\begin{aligned}
\Delta E_{\mathrm{cm}}(p_{\mathrm{beam}}) &= \sqrt{\left(\frac{\partial E_{\mathrm{cm}}}{\partial p_{\mathrm{beam}}} \cdot \Delta p_{\mathrm{beam}}\right)^2} = \left|\frac{\partial E_{\mathrm{cm}}}{\partial p_{\mathrm{beam}}} \cdot \Delta p_{\mathrm{beam}}\right| = \left|\frac{\partial E_{\mathrm{cm}}}{\partial p_{\mathrm{beam}}}\right| \cdot |\Delta p_{\mathrm{beam}}| \\
&= \left| \underbrace{\frac{1}{2} \cdot \left(2m_{\mathrm{p}}^2 + 2m_{\mathrm{p}} \cdot \sqrt{m_{\mathrm{p}}^2 + {p_{\mathrm{beam}}}^2}\right)^{-\frac{1}{2}} \cdot 2m_{\mathrm{p}} \cdot \frac{1}{2} \cdot (m_{\mathrm{p}}^2 + {p_{\mathrm{beam}}}^2)^{-\frac{1}{2}} \cdot 2p_{\mathrm{beam}}}_{>0} \right| \cdot \left| \underbrace{\Delta p_{\mathrm{beam}}}_{>0} \right| \\
&= \left(\frac{m_{\mathrm{p}} \cdot p_{\mathrm{beam}}}{\sqrt{2m_{\mathrm{p}}^2 + 2m_{\mathrm{p}} \cdot \sqrt{m_{\mathrm{p}}^2 + {p_{\mathrm{beam}}}^2}} \cdot \sqrt{m_{\mathrm{p}}^2 + {p_{\mathrm{beam}}}^2}} \right) \cdot \Delta p_{\mathrm{beam}} \\
&= \frac{m_{\mathrm{p}} \cdot p_{\mathrm{beam}}}{\sqrt{2m_{\mathrm{p}}^2 \cdot (m_{\mathrm{p}}^2 + {p_{\mathrm{beam}}}^2) + 2m_{\mathrm{p}} \cdot \sqrt{m_{\mathrm{p}}^2 + {p_{\mathrm{beam}}}^2}^3}} \cdot \Delta p_{\mathrm{beam}}
\end{aligned}
\tag{26}
$$

[15] This simplified estimate is in agreement with section 2.4.4 of [27]. See section 7 for a discussion of alternative methods of estimating the center of mass energy distribution.

Using equation (26) to exemplarily calculate ΔE_{cm} for $p_{\mathrm{beam}} = 6.988$ GeV yields

$$\Delta E_{\mathrm{cm}}(6.988 \text{ GeV}) \simeq 33.568 \text{ keV}. \tag{27}$$

With equation (13) the full width at half maximum of the center of mass energy distribution can be calculated. The result is: $\mathrm{FWHM}(\Delta E_{\mathrm{cm}}(6.988 \text{ GeV})) = \sqrt{8\ln(2)} \cdot 33.568 \text{ keV} \simeq 79.047$ keV. Even though the obtained value represents a rather small uncertainty in E_{cm}, a sophisticated resonance scan simulation has to take the beam momentum spread and the E_{cm} dependency of the cross section for X(3872) formation into account. More details on the simulation procedure can be found in section 6.4.1.

While direct production in e^+e^- collisions is limited to resonances with quantum numbers $J^{PC}=1^{--}$ due to the intermediate virtual photon, in $p\overline{p}$ collisions states of all non-exotic quantum numbers can be formed. Exotic J^{PC} states can for instance be produced in association with a pion [31]. The X(3872) has positive C parity and therefore, it cannot be directly produced in e^+e^-. If it had a spin of 2 and was a charmonium state, it could be produced via two-photon formation $\gamma\gamma \to c\bar{c}$ in e^+e^- colliders, but the luminosity for such processes decreases approximately with the inverse mass of the state. According to [8], the favored quantum number assignment of $J^{PC}=1^{++}$ prohibits a two-photon formation in e^+e^- assuming the X(3872) was a $c\bar{c}$ state.

A production in hadronic collisions usually comes at the cost of a huge background and only decays to $\mu^+\mu^-$ could be favorable candidates for analyses [8]. $p\overline{p}$ collisions should be much cleaner and therefore, HESR with its cooled antiproton beam should be the best choice as a laboratory for an investigation of the X(3872) cross section as a function of the center of mass energy with a resonance scan which is explained in section 4.3.

4.3. Resonance Scan

Performing a resonance scan is a powerful technique to measure resonance parameters with high precision which is an important part of the $\overline{\text{P}}$ANDA physics programme. This method is very suitable to determine masses, widths and decay fractions by scanning the center of mass energy E_{cm} across the resonance of interest by adjusting the beam momentum p_{beam}. The Fermilab experiments E760 and E835 pioneered this technique using antiproton beams and internal targets. The authors of [32] were able to determine the width of the J/ψ to $\Gamma_{J/\psi} = 99 \pm 12(\text{stat.}) \pm 6(\text{syst.})$ keV and the width of the ψ' to $\Gamma_{\psi'} = 306 \pm 36(\text{stat.}) \pm 16(\text{syst.})$ keV. The beam momentum resolution available for those measurements was $\Delta p/p \leq 2 \cdot 10^{-4}$ which according to [32] corresponds to a full width at half maximum (FWHM) center of mass resolution of roughly 0.5 MeV for the observed shape of the momentum distribution. For $\overline{\text{P}}$ANDA $\Delta p/p$=$2{\cdot}10^{-5}$ is aimed at with HESR in high resolution mode which should yield about a factor of ten better center of mass energy resolution than the Fermilab experiments had available. Assuming a Gaussian beam momentum spread for HESR the center of mass energy will be approximately Gaussian distributed with a FWHM center of mass energy resolution of about 79 keV at $E_{\text{cm}} = m_{\text{X(3872)}}$ (see section 4.2).

As mentioned in section 4.2 $\text{p}\overline{\text{p}}$ annihilations are very suitable for this experimental method, because resonances of all non-exotic quantum numbers can be formed directly and in a resonance scan the center of mass energy E_{cm} is determined by the known nominal antiproton momentum while the detector is only used for counting the events.

The $\overline{\text{P}}$ANDA detector will feature good particle identification and in combination with the precisely-calibrated and cooled antiproton beam from HESR an unprecedented precision will be feasible.

4.4. The PandaRoot Framework

PandaRoot [33] is the official software framework of the $\overline{\text{P}}$ANDA collaboration and can be used with more than 15 Linux platforms. It is based on CERN's root [34] and will include all $\overline{\text{P}}$ANDA subdetectors which corresponds to about 43,000 detailed geometry volumes also including details such as the target pipe, as well as detailed magnetic field maps. PandaRoot consists of more than 400,000 lines of C++ code. The transport engines Geant3, Geant4, and Fluka are built-in. As event generators, EvtGen, DPM, PYTHIA, and UrQMD are available. References to the mentioned software and more information on PandaRoot can be found in [35] and in section 3 of [27].

In this work the PandaRoot framework is used to carry out all steps necessary for a resonance scan of the X(3872) from simulation and transport to digitization, reconstruction and analysis. The tasks and purposes of the most important scripts and PandaRoot macros utilized in this work is outlined in appendix C.

Figure 6 shows a screen shot of the PandaRoot event display presenting a signal event $\text{p}\overline{\text{p}} \to \text{X(3872)} \to J/\psi\ \pi^+\pi^-$ with a subsequent decay $J/\psi \to \text{e}^+\text{e}^-$ for the resonance scan simulation.

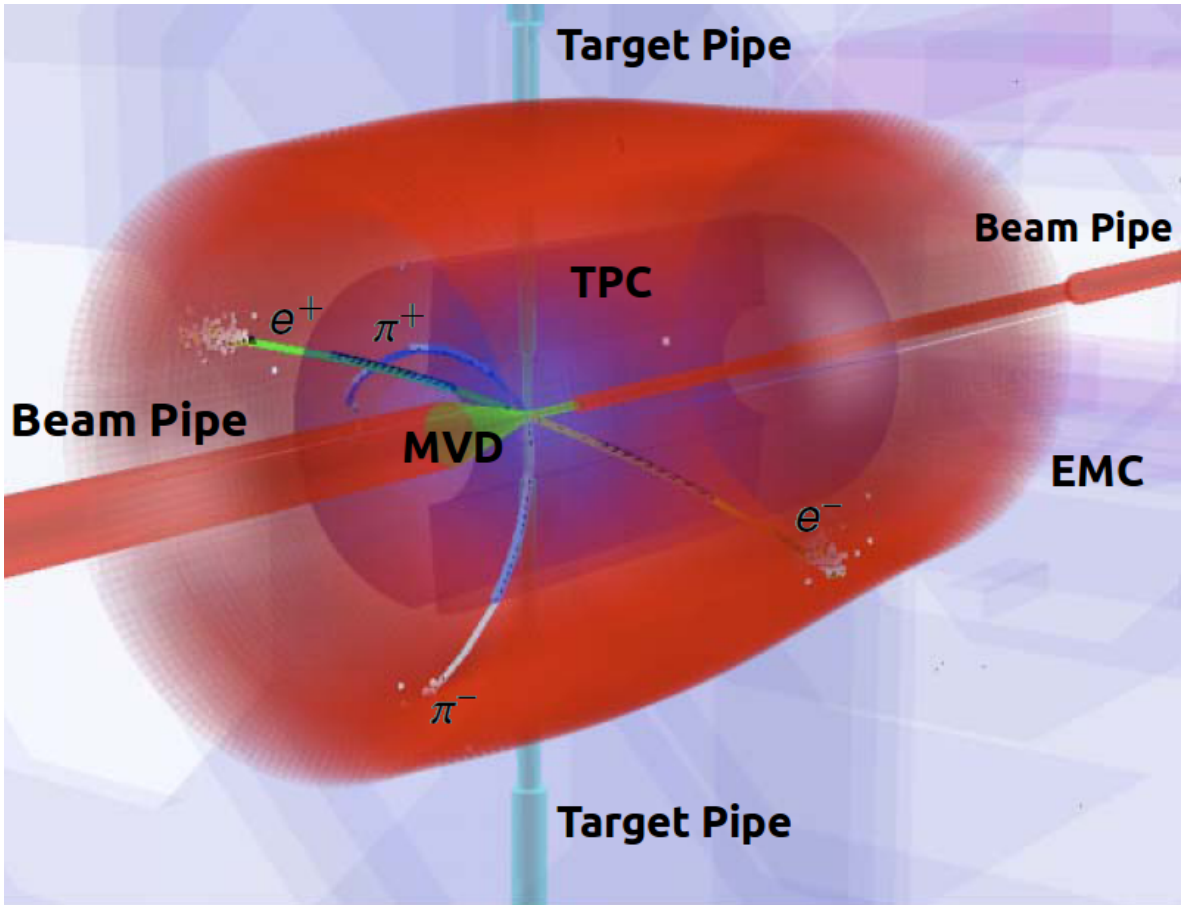

Figure 6: A view into the inner part of $\overline{\mathrm{P}}$ANDA's target spectrometer is shown. The PandaRoot event display shows the reconstructed tracks of the decay products of a simulated signal event $\mathrm{p\overline{p}} \to \mathrm{X}(3872) \to J/\psi\ \pi^+\pi^-$ with a subsequent $J/\psi \to \mathrm{e^+e^-}$ decay. Labels were added to denote the subdetectors as well as the decay particles' tracks.

5. Simulation Parameters and Estimates

5.1. Estimated Rates for X(3872) Formation at $\overline{\text{P}}$ANDA

The cross section for X(3872) production in $\text{p}\overline{\text{p}}$ annihilations is currently unknown. Also the width and the branching ratio for the time inverse process X(3872) $\rightarrow \text{p}\overline{\text{p}}$ are unknown. In order to carry out the simulation of a resonance scan certain a cross section $\sigma[\text{p}\overline{\text{p}} \rightarrow \text{X}(3872)] = 50$ nb is assumed[16]. This estimate is of the same order of magnitude as for instance the according ψ' cross section [32]. It is also consistent with the predictions in [2] for relatively large widths $\Gamma_{\text{X}(3872)}$. However, in the simulation $\Gamma_{\text{X}(3872)}$ is chosen to be 100 keV. Combining a very narrow width and a relatively small cross section is a rather pessimistic estimate for the simulation parameters and can be regarded as a worst case scenario. If the model calculations in [2] are correct, either the true width should be significantly larger for the assumed cross section or in case the true width $\Gamma_{\text{X}(3872)}$ is close to 100 keV, the total cross section should be significantly larger than the chosen value of 50 nb. If future measurements lead to new or improved information on the characteristics of the X(3872), the simulation can easily be carried out with adjusted parameters, because the entire simulation chain is highly automated using a combination of bash shell scripts and PandaRoot macros. The simulation parameters can conveniently be adjusted in a central script which was created for this thesis and controls almost the entire simulation chain without any need for human intervention.

For the simulation of the resonance scan it is important to know how many signal events have to be simulated for each scan point. This number can be calculated using equation (22). The numerical integration of the effective cross section given by equation (23) using the determined uncertainty $\Delta E_{\text{cm}} \simeq 33.568$ keV of the approximately Gaussian center of mass energy distribution – which was calculated in section 4.2 for HESR in the high resolution mode – gives

$$\sigma_{\text{eff}}(m_{\text{X}(3872)}) \simeq 38.6 \text{ nb}. \tag{28}$$

This is the effective cross section for X(3872) production with HESR in high resolution mode at a nominal center of mass energy $E_{\text{cm}0} = m_{\text{X}(3872)}$. Such numerical integrations have to be carried out for each scan point to estimate the number of signal events that need to be simulated. In the following the estimate is exemplarily carried out for a hypothetical scan point in which the nominal center of mass energy is equal to the mass of the X(3872).

The decay channel of interest is X(3872) $\rightarrow J/\psi\ \pi^+\pi^-$ and the ratio of branching fractions $[J/\psi\ \pi^+\pi^- : D^0\bar{D}^{*0}\text{: other}]$ is assumed to be approximately $[1 : 9 : 0]$. This yields an effective cross section $\sigma_{\text{eff}}[\text{p}\overline{\text{p}} \rightarrow \text{X}(3872) \rightarrow J/\psi\ \pi^+\pi^-]$ of 3.86 nb.

The J/ψ can be reconstructed from its decays to e^+e^- and $\mu^+\mu^-$. As the branching fractions for $J/\psi \rightarrow \text{e}^+\text{e}^-$ and for $J/\psi \rightarrow \mu^+\mu^-$ are about 6% [1] each, the cross section into the reconstructed decay channel is about 463.2 pb.

[16] $\sigma[\text{p}\overline{\text{p}} \rightarrow \text{X}(3872)]$ is more accurately written as $\sigma_{\text{BW}}[\text{p}\overline{\text{p}} \rightarrow \text{X}(3872) \rightarrow \text{all}](m_{\text{X}(3872)})$ and interpreted as explained in section 3.5. See section 5.2 for a calculation of the branching ratio BR(X(3872) $\rightarrow \text{p}\overline{\text{p}}$) from the parameters chosen for the resonance scan simulation.

Running HESR in its high resolution mode with $\Delta p_{\mathrm{beam}}/p_{\mathrm{beam}} \leq 2 \cdot 10^{-5}$ yields a design luminosity of $\mathcal{L} = 2 \cdot 10^{31}\ \mathrm{cm}^{-2}\mathrm{s}^{-1}$ (see table 3). As the following calculation shows, this corresponds to an integrated luminosity $\mathcal{L}_{\mathrm{int}}$ of 0.864 pb^{-1}/day with an estimated accelerator duty factor α of 50%.

$$\begin{aligned}
\mathcal{L}_{\mathrm{int}} = \frac{\int \mathcal{L} \cdot \alpha \ \mathrm{dt}}{1\ \mathrm{day}} &= 2 \cdot 10^{31}\ \mathrm{cm}^{-2} \cdot 1\ \mathrm{s}^{-1} \cdot \frac{1}{2} \cdot \frac{60\ \mathrm{s}}{1\ \mathrm{min}} \cdot \frac{60\ \mathrm{min}}{1\ \mathrm{h}} \cdot \frac{24\ \mathrm{h}}{1\ \mathrm{day}} \\
&= 10^{31} \cdot (10^{-2})^{-2}\ \mathrm{m}^{-2} \cdot \underbrace{\frac{60}{1} \cdot \frac{60}{1} \cdot \frac{24}{1\ \mathrm{day}}}_{8.64 \cdot 10^4/\mathrm{day}} \\
&= 8.64 \cdot 10^{39} \cdot \frac{10^{-12} \cdot 10^{-28}}{10^{-12} \cdot \underbrace{10^{-28}\ \mathrm{m}^2}_{1\ \mathrm{b}=10^{-28}\ \mathrm{m}^2}}\ \mathrm{per\ day} \\
&= 8.64 \cdot \frac{10^{-1}}{1\ \mathrm{pb}}\ \mathrm{per\ day} = 0.864\ \mathrm{pb}^{-1}\ \mathrm{per\ day} \qquad (29)
\end{aligned}$$

For a resonance scan with 20 energy points and 2 days per scanpoint about 400 signal events of $\mathrm{p\overline{p}} \to \mathrm{X}(3872) \to J/\psi\ \pi^+\pi^-$ need to be simulated for a scanpoint with $E_{\mathrm{cm}} = m_{\mathrm{X}(3872)}$. With a reconstruction efficiency $\epsilon \simeq 50\%$ about 200 reconstructed signal events per simulated day of data taking should be measured as the following calculation shows.

$$n_{\mathrm{measured\ signals}}\ \mathrm{per\ day} = 0.864\ \frac{1}{\mathrm{pb}} \cdot \frac{1}{\mathrm{day}} \cdot 463.2\ \mathrm{pb} \cdot 0.5 \simeq 200\ \mathrm{per\ day}.$$

It appears rather unrealistic that a real experiment would adjust the average beam momentum such that the center of mass energy matches exactly the maximum of the true X(3872) Breit-Wigner distributed cross section. Therefore, a small energy shift $\Delta E = 10$ keV is assumed. This value describes how much the closest scan point's energy is separated from the true X(3872) mass.

It is feasible to perform the resonance scan in a way that about half the scan points are at energies greater than $m_{\mathrm{X}(3872)}$ and the other half is below $m_{\mathrm{X}(3872)}$. This scenario is assumed in the simulation. The results of the simulated resonance scan are presented and discussed in section 6.4.

5.2. Estimation of BR(X(3872) → pp̄)

In section 5.1 the assumption was made that the cross section for the process $\mathrm{p\overline{p}} \to \mathrm{X}(3872)$ is 50 nb for a monoenergetic center of mass energy equal to the X(3872) mass. From this assumption an estimate for the branching ratio $\mathrm{BR}(\mathrm{p\overline{p}} \to \mathrm{X}(3872))$ can be obtained which other experiments – for instance the Belle collaboration with their large data set in a work similar to [36] – could assess.

As noted in section 3.5 resonant cross sections are generally described by the Breit-Wigner formula which is given for the special case of resonance production in $\mathrm{p\overline{p}}$ annihilations in equation (20). As final state f all possible decay channels are considered. Therefore, $\mathrm{BR}(\mathrm{X}(3872) \to f)$ is equal to 1. The assumed cross section is denoted by $\sigma[\mathrm{p\overline{p}} \to \mathrm{X}(3872)]$ and more accurately written as $\sigma_{\mathrm{BW}}[\mathrm{p\overline{p}} \to \mathrm{X}(3872) \to \mathrm{all}](m_{\mathrm{X}(3872)})$ which can be written more explicitly using the Breit-Wigner formula (20):

$$\begin{aligned}
\sigma[\mathrm{p\overline{p}} \to \mathrm{X}(3872)] \quad &= \quad \sigma_{\mathrm{BW}}[\mathrm{p\overline{p}} \to \mathrm{X}(3872) \to \mathrm{all}](m_{\mathrm{X}(3872)}) \\
&\overset{\text{eq. (20)}}{=} \quad \frac{(2 \cdot J + 1) \cdot 4\pi}{{m_{\mathrm{X}(3872)}}^2 - 4m_{\mathrm{p}}^2} \cdot \frac{\mathrm{BR}(\mathrm{X}(3872) \to \mathrm{p\overline{p}}) \cdot \overbrace{\mathrm{BR}(\mathrm{X}(3872) \to f)}^{=1} \cdot {\Gamma_{\mathrm{X}(3872)}}^2}{\underbrace{4(m_{\mathrm{X}(3872)} - m_{\mathrm{X}(3872)})^2}_{=0} + {\Gamma_{\mathrm{X}(3872)}}^2} \\
&\overset{(J=1)}{=} \quad \frac{3 \cdot 4\pi}{{m_{\mathrm{X}(3872)}}^2 - 4m_{\mathrm{p}}^2} \cdot \mathrm{BR}(\mathrm{X}(3872) \to \mathrm{p\overline{p}}) \qquad (30)
\end{aligned}$$

Equation (30) can be solved for $\mathrm{BR}(\mathrm{X}(3872) \to \mathrm{p\overline{p}})$:

$$\begin{aligned}
\mathrm{BR}(\mathrm{X}(3872) \to \mathrm{p\overline{p}}) &= \sigma[\mathrm{p\overline{p}} \to \mathrm{X}(3872)] \cdot \frac{{m_{\mathrm{X}(3872)}}^2 - 4m_{\mathrm{p}}^2}{3 \cdot 4\pi} \\
&\overset{*}{=} 50 \text{ nb} \cdot \frac{3.872^2 - 4 \cdot 0.938272013^2}{12\pi} \cdot \frac{1 \text{ GeV}^2}{389379.304 \text{ nb GeV}^2} \\
&\simeq 3.9 \cdot 10^{-5} \qquad (31)
\end{aligned}$$

In the marked step of the calculation the conversion of units from section 5.1

$$1 = 389379.304 \text{ nb GeV}^2$$

was employed to express the result of the Breit-Wigner formula in nanobarn. For the simulation the X(3872) was assumed to have spin $J = 1$, mass $m_{\mathrm{X}(3872)} = 3.872$ GeV and full width at half maximum $\Gamma_{\mathrm{X}(3872)} = 100$ keV. The latter is used to estimate the partial width for $\mathrm{X}(3872) \to \mathrm{p\overline{p}}$:

$$\begin{aligned}
\Gamma_{\mathrm{X}(3872)}(\mathrm{X}(3872) \to \mathrm{p\overline{p}}) &= \mathrm{BR}(\mathrm{X}(3872) \to \mathrm{p\overline{p}}) \cdot \Gamma_{\mathrm{X}(3872)} \\
&\simeq 3.9 \cdot 10^{-5} \cdot 100 \text{ keV} = 3.9 \text{ eV} \qquad (32)
\end{aligned}$$

The properties of X(3872) which were assumed in this work can now be checked for consistency by setting upper or lower limits on the branching ratio or partial width for $\mathrm{X}(3872) \to \mathrm{p\overline{p}}$ for instance with $\mathrm{e^+e^-}$ colliders. The obtained results (31) and (32) need to be within such limits to be compatible with nature and can be adjusted if necessary.

5.3. Background Estimation

A detailed Monte Carlo simulation of the background is very important in order to determine the feasibility of a resonance scan of the X(3872) excitation curve with $\overline{\mathsf{P}}$ANDA. The expected accuracy of the obtained physical results strongly depends on the signal to background ratio as well as on the background suppression capabilities of the detector.

For the resonance scan simulation of X(3872) mainly the following possible sources for background need to be considered:

Combinatoric background occurs when multiple entities of the same particle type – which originated from different decays – are present in the same event. Consider the final state $J/\psi\ \pi^+\pi^-$ with a subsequent J/ψ decay into $\mu^+\mu^-$. Charged pions decay almost entirely into muons of the according charge and a muon neutrino or antineutrino. As it is unknown which $\mu^+\mu^-$ pair originated from the J/ψ decay, such an event could lead to combinatoric background when J/ψ reconstruction by calculating the invariant mass of two oppositely charged muons is attempted.

However, combinatoric backgroud has hardly any significance for the final state of interest, because $c\tau$ ($\simeq 7.8$ m [1]) for charged pions is sufficiently large, so that most of them are measured by the detector before they decay into muons. Muons have an even longer lifetime with $c\tau \simeq 658.7$ m and almost all muons are measured before they decay nearly exclusively into electrons or positrons and the according electronic (anti-)neutrinos.

Therefore, typical formation of X(3872) and the decay into $J/\psi\ \pi^+\pi^-$ events contain only four charged particles. The J/ψ is detected from its decay into long-lived $\mu^+\mu^-$ or stable $\mathrm{e}^+\mathrm{e}^-$. Only if a J/ψ can be reconstructed it is attempted to calculate the invariant mass of X(3872) candidates by adding the two relatively long-lived pions which are measured directly by the detector.

Separation of events can be an experimental challenge, especially when using a TPC in combination with high rates, because the long drift times make it hard to determine which measured particle belongs to which event. Pile-ups of several 100 events may occur. This is of course partially alleviated by choosing to run HESR in the high resolution mode.

Decays of other resonances into the same final state $J/\psi\ \pi^+\pi^-$ has a negligible effect, because the X(3872) mass is rather well separated from states with such decay channels. For instance, ψ' and ψ'' both decay into $J/\psi\ \pi^+\pi^-$, but can only be produced in association with another light particle or for instance when initial state radiation occurs. As $\overline{\mathsf{P}}$ANDA features a solid angle coverage of almost 4π, it should be possible to reject according background events. Therefore, such background is neglected in this work.

The direct process $\mathrm{p\overline{p}} \to J/\psi\ \pi^+\pi^-$ in which the investigated final state is reached without the intermediate X(3872) formation and decay cannot be kinematically distinguished from the signal. In [2] it is estimated that the background from the direct reaction

should be nearly constant in the center of mass energy around the mass of the X(3872). A constant cross section $\sigma[\mathrm{p\overline{p}} \to J/\psi\ \pi^+\pi^-]$ of 1.2 nb is assumed for the simulation which corresponds to 1036.8 events per day for this background channel.

$$\begin{aligned} n_{\mathrm{p\overline{p}}\to J/\psi\ \pi^+\pi^-}\ \text{per day} &= 0.864\ \frac{1}{\text{pb}} \cdot \frac{1}{\text{day}} \cdot 1.2\ \text{ nb} \\ &= 0.864\ \frac{1}{10^{-12}\ \text{b}} \cdot \frac{1}{\text{day}} \cdot 1.2 \cdot 10^{-9}\ \text{b} \\ &= 1036.8\ \text{per day} \end{aligned} \tag{33}$$

If the estimates in [2] are correct, the signal should be visible on top of a nearly constant background from this direct background.

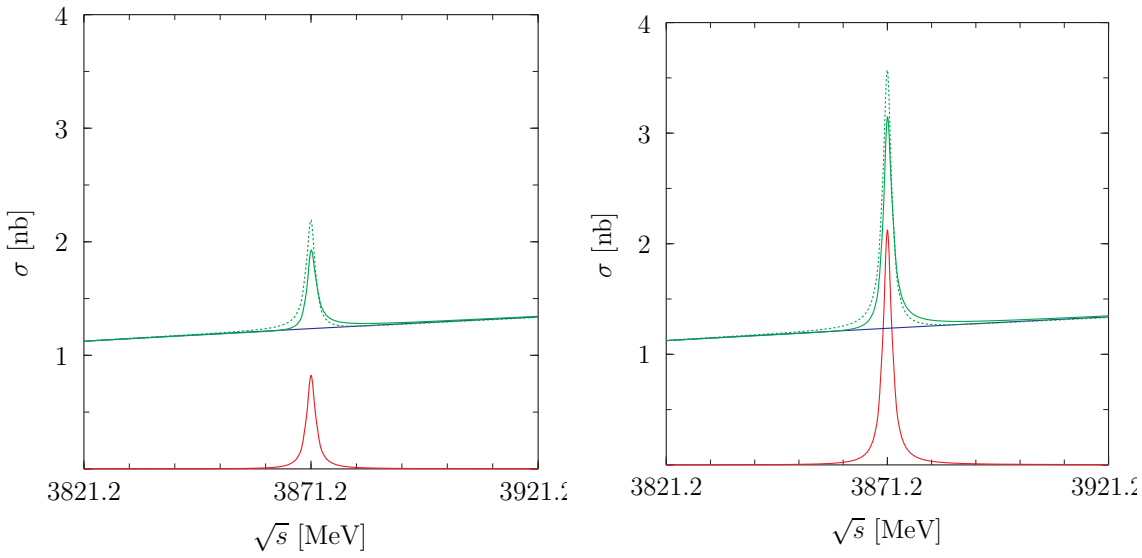

Figure 7: Plots of the predicted total cross section $\sigma[\mathrm{p\overline{p}} \to \mathrm{X}(3872) \to J/\psi\pi^+\pi^-]$ as a function of the center of mass energy $\sqrt{s}$ for the X(3872) as $\chi_{c1}(2P)$ (left plots) and for X(3872) as a loosely bound state of D-mesons (right hand side) are shown. The lower curves correspond to cross sections for the signal only. The upper curves include background from the process $\mathrm{p\overline{p}} \to J/\psi\ \pi^+\pi^-$ which leads to the same final state, but without the intermediate X(3872) formation and decay. The solid and dashed curves represent two different scenarios for the calculation performed in [2]. The plots were taken from that paper.

Processes that end up in final states which are similar to the signal are the most important type of background to investigate. For a detailed study of this kind of background, PandaRoot's built-in dual parton model (DPM [37]) event generator is used.

The main background is expected to come from the process $\mathrm{p\overline{p}} \to \pi^+\pi^-\pi^+\pi^-$ in which one pion of each charge is misidentified as a lepton. The cross section for this process is about $\sigma_{\mathrm{BG}} \simeq 50\ \mu\mathrm{b}$ [38] in the region of $\overline{\mathrm{p}}$-beam momentum $p_{\mathrm{beam}} \simeq 6.988$ GeV which is required for a center of mass energy E_{cm} in the region of the X(3872) mass (see equation (18)).

A broader approach is to investigate all inelastic background events. Assuming a 100% suppression of elastic events, the total $p\overline{p}$ inelastic cross section for the relevant p_{beam} region can be obtained from subtracting the elastic $p\overline{p}$ cross section of roughly 15 mb from the total $p\overline{p}$ cross section of about 60 mb. Both values were read off the plot shown in figure 8 which was found in [1]. Compared to an estimated signal cross section of about 463.2 pb this is a huge cross section.

An estimate on the number of background events per day can be obtained using the result from equation (29) for the integrated luminosity of 0.864 pb^{-1} per day.

$$\begin{aligned} n_{\pi^+\pi^-\pi^+\pi^-} \text{ per day} &= 0.864 \ \frac{1}{\text{pb}} \cdot \frac{1}{\text{day}} \cdot 50 \ \mu\text{b} \\ &= 0.864 \ \frac{1}{10^{-12} \text{ b}} \cdot \frac{1}{\text{day}} \cdot 50 \cdot 10^{-6} \text{ b} \\ &= 4.32 \cdot 10^7 \text{ per day} \qquad (34) \\ n_{\text{inelastic}} \text{ per day} &= 0.864 \ \frac{1}{\text{pb}} \cdot \frac{1}{\text{day}} \cdot (60 - 15) \text{ mb} \\ &= 0.864 \ \frac{1}{10^{-12} \text{ b}} \cdot \frac{1}{\text{day}} \cdot 35 \cdot 10^{-3} \text{ b} \\ &= 3.024 \cdot 10^{10} \text{ per day} \qquad (35) \end{aligned}$$

As one scan point will correspond to two days of data taking, the obtained values from equation (34) and (35) have to be multiplied by a factor of two to get the approximate total amount of background events that occur during data taking for one scan point.

See section 6.3 for a discussion of these numbers.

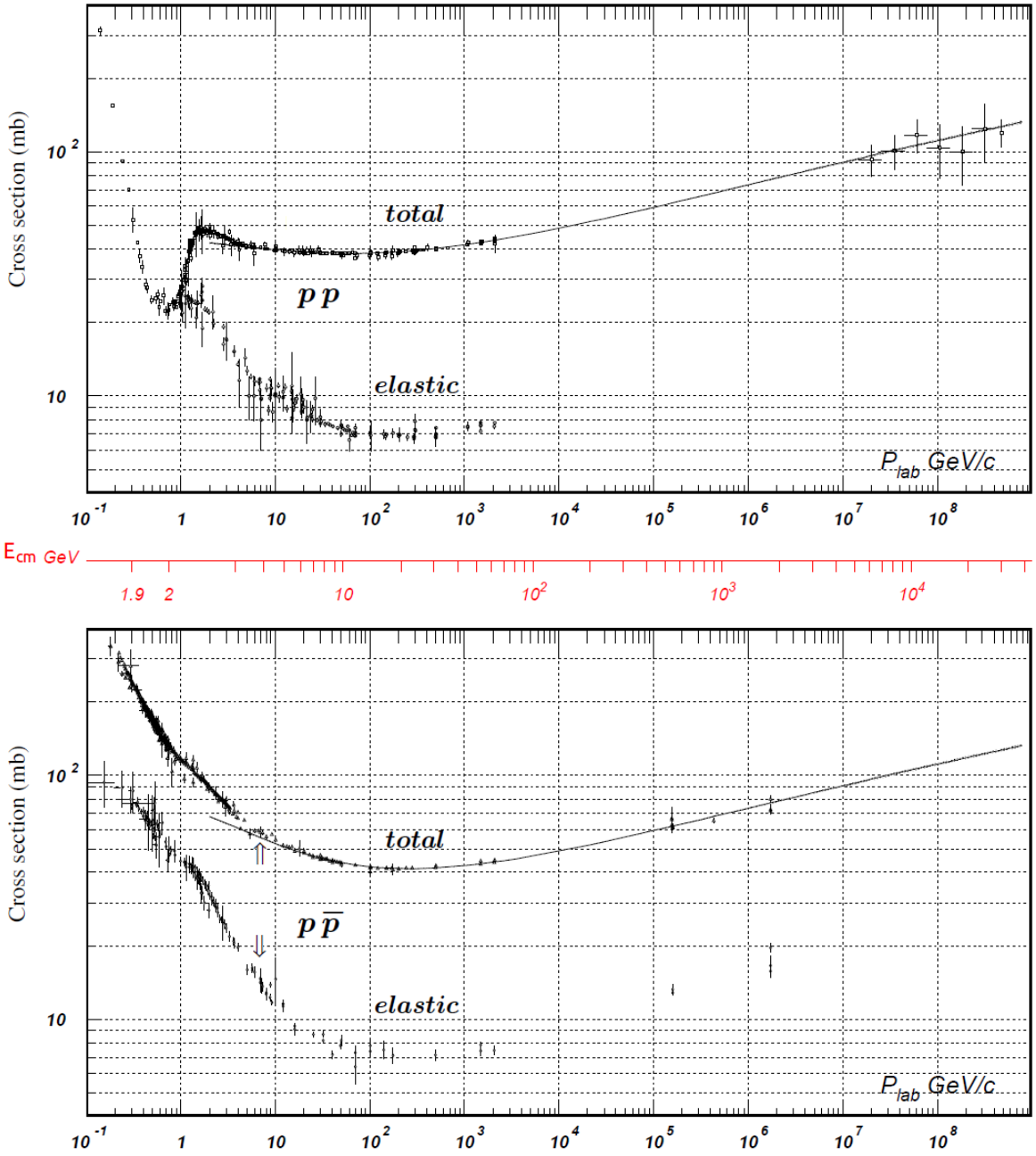

Figure 8: Plots of total and elastic cross sections for proton-proton- (p p) and proton-antiproton- (p $\overline{\text{p}}$) collisions as a function of laboratory beam momentum (p_{lab}) and total center-of-mass energy (E_{cm}) as found in [1]. The labels have been adapted to comply with the notation used in this thesis and two arrows were added to indicate the values which were read off the plots.

6. Results from PandaRoot Simulation

The Monte Carlo simulations presented in this work were entirely carried out using the PandaRoot framework – which is outlined in section 4.4 – and the software written for this thesis – which is documented in appendix C. All simulations were computed on the cluster described in appendix D.

For the simulations the most important $\overline{\mathsf{P}}$ANDA target spectrometer detectors are included (see detector setup code in appendix B), but the reconstruction uses only the following subdetectors:

- The Micro Vertex Detector with 120 silicon pixel modules – with a pixel size of 100×100 μm^2 and 10 million readout channels – and 400 silicon strip modules – with an active area of about 0.5 m^2 and 7,000 readout channels.

- The time projection chamber with 135 padrows which yield up to 135 hits for a single track of a charged particle and 135,169 pads of 2×2 mm^2 area.

- The electromagnetic calorimeter with approximately 17,200 fast lead-tungstate crystals with a thickness of about 28 radiation lengths.

Detailed magnetic field maps of the homogenous $B_z = 2$ T field produced by the target spectrometer's solenoid and the dipole field with 2 Tm bending power in the forward region are taken into accout by PandaRoot. The same is true for flux effects in the iron of the $\overline{\mathsf{P}}$ANDA muon subdetector and the interference of the fields. Conformal map based track finder and track fitter algorithms are used for pattern recognition to achieve a realistic signal reconstruction.

For the simulation of the formation and subsequent decay of X(3872) *EvtGen* [39] is used as event generator. Final state radiation using the PHOTOS software package [40] is simulated. The inelastic hadronic background is simulated using the DPM (dual parton model) generator mentioned in section 5.3. After the generation of events, background and signal events are treated exactly the same: The particles are transported through the geometry of the $\overline{\mathsf{P}}$ANDA detector using Geant3 [41, 42]. The digitization, reconstruction and particle identification is carried out in the PandaRoot framework. The analysis treats the output of the simulation like real data.

6.1. Signal: $p\overline{p} \to X(3872) \to J/\psi\ \pi^+\pi^-$

For the results in this section 5000 Monte Carlo events of $p\overline{p} \to X(3872) \to J/\psi\ \pi^+\pi^-$ with subsequent J/ψ decays to e^+e^- and 5000 events with subsequent J/ψ decays to $\mu^+\mu^-$ were simulated using PandaRoot revision 8466. For the X(3872) a decay model of a vector resonance decaying into a vector particle and two pions was used which is abbreviated by *VVPiPi*. For the J/ψ the model *VLL* was chosen which describes the decay of a vector particle into two leptons.

As a first step to the simulation of an X(3872) resonance scan, the decay channel of interest $J/\psi\ \pi^+\pi^-$ has to be studied. It was decided that the J/ψ should be reconstructed by its decay into e^+e^- or $\mu^+\mu^-$.

A cut on the invariant mass of two oppositely charged particles – which is shown in the upper left plot in figure 9 for the decay of $J/\psi \to e^+e^-$ and on the upper right plot for $J/\psi \to \mu^+\mu^-$ – is applied to reject background. The only particle identification (PID) information used in this section is the particles' charges. Their momenta are reconstructed from MVD and TPC measurements.

A cut on the missing mass of two oppositely charged particles is applied as well. The cut region from 2.7 GeV to 3.6 GeV is indicated in the lower plot on the right hand side of figure 9.

Only combinations of J/ψ candidates and $\pi^+\pi^-$ candidates – which satisfy the aforementioned conditions – are used to calculate the invariant mass of four charged particles which is displayed in the lower left plot. Double counting is excluded by requiring that for every X(3872) candidate none of the two particles that are used to reconstruct the J/ψ candidate is used to calculate the missing mass of pion candidats. Out of 5000 simulated signal events of $p\overline{p} \to X(3872) \to J/\psi\ \pi^+\pi^-$ with subsequent J/ψ decays to $\mu^+\mu^-$, about 3400 X(3872) candidates in the appropriate mass region are obtained. The efficiency for subsequent J/ψ decays into e^+e^- is slightly lower ($\simeq$ 3200 X(3872) candidates) due to final state radiation which can clearly be seen as a radiative tail in the two particle invariant mass in the upper left plot. An additional photon is radiated in about 30% of all simulated $J/\psi \to e^+e^-$ decays.

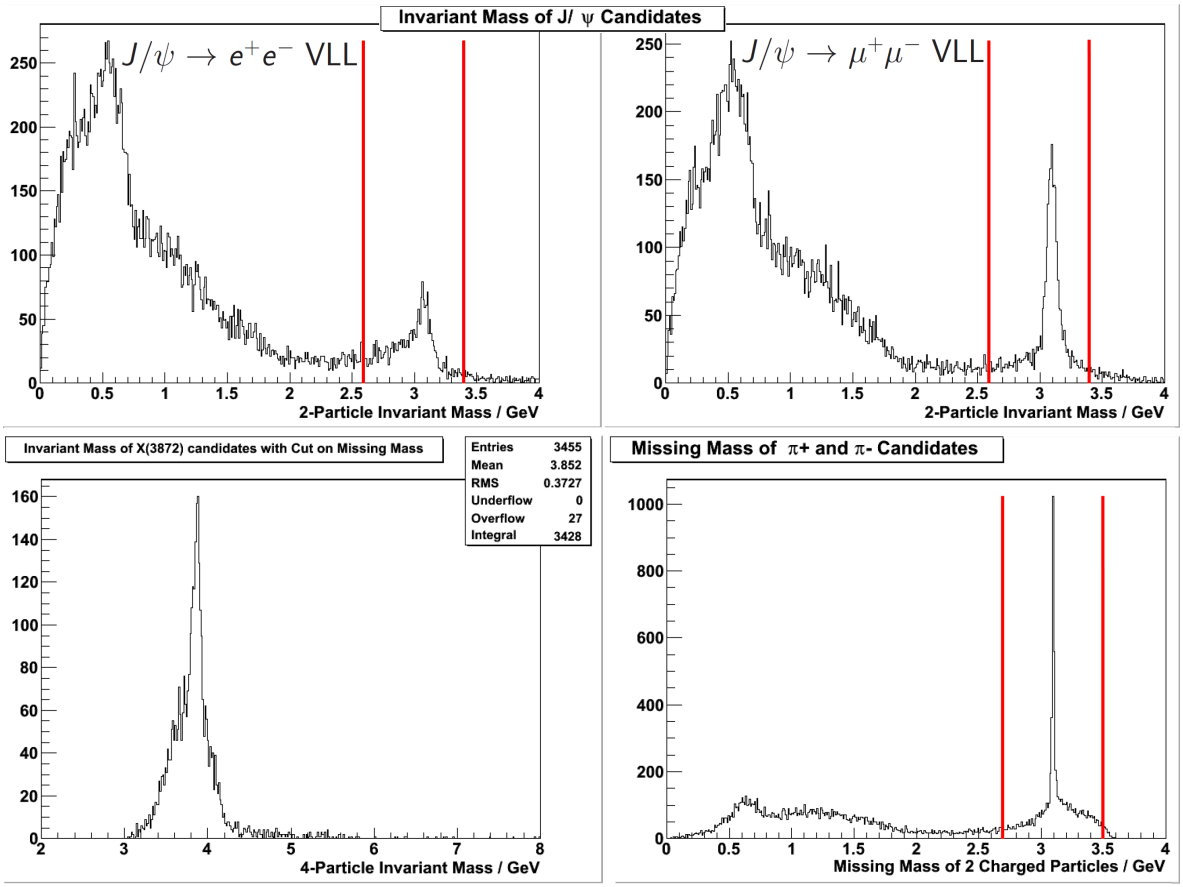

Figure 9: Plots of 5000 simulated $p\overline{p} \to X(3872) \to J/\psi\ \pi^+\pi^- \to e^+e^-\ \pi^+\pi^-$ and 5000 $p\overline{p} \to X(3872) \to J/\psi\ \pi^+\pi^- \to \mu^+\mu^-\ \pi^+\pi^-$ events are shown.

Upper left/right: Invariant mass plot of two oppositely charged particles for $J/\psi \to e^+e^-$ / $J/\psi \to \mu^+\mu^-$ using the VLL decay model.

Lower right: The missing mass of all combinations of two oppositely charged particles is plotted for a subsequent J/ψ decay to $\mu^+\mu^-$. The according plot for the e^+e^- case looks very similar.

Lower left: Four particle invariant mass spectrum for combinations of $\mu^+\mu^-$ which yield a J/ψ candidate within the J/ψ mass cut region and $\pi^+\pi^-$ candidates with a missing mass within the admissible J/ψ mass region.

The respective mass cut regions are indicated by two vertical red lines. For more details refer to the text.

6.2. Electron / Pion Discrimination Using $E_{\mathbf{EMC}}/p$

For the analysis of an X(3872) resonance scan with final state $J/\psi\ \pi^+\pi^-$ and subsequent J/ψ decay into e^+e^- or $\mu^+\mu^-$, it is important to be able to discriminate at least between charged pions, muons and electrons/ positrons.

A straightforward approach is to use the ratio of a charged particle's shower energy E_{EMC} deposited in the EMC and its momentum p – which is determined by the track finder and track fitter using the MVD and the TPC information. This method requires the matching of charged particle tracks reconstructed from MVD and TPC measurements and clusters measured in the EMC.

Three different simulations corresponding to the three different particle types $e^\pm$, $\mu^\pm$ and $\pi^\pm$ were carried out using PandaRoot revision 8466 to determine how a cut on the variable E_{EMC}/p could be applied:

$\mu^\pm$: As a muon source the process $J/\psi \to \mu^+\mu^-$ using the vector to two leptons (VLL) decay model was chosen.

$e^\pm$: The same decay model is applied to $J/\psi \to e^+e^-$ which is utilized as a source for high energy $e^\pm$.

$\pi^\pm$: For the process $\psi(2S) \to J/\psi\ \pi^+\pi^-$ the VVPiPi decay model is used and the subsequent J/ψ decay is prohibited in EvtGen to receive a clean source of charged pions in the appropriate energy regime.

The resulting distributions of E_{EMC}/p for the aforementioned simulations are presented in figure 10. The simulation leads to the following observations:

High energy $e^\pm$ pairs which come from J/ψ decays create electromagnetic showers in the EMC. The according E_{EMC}/p distribution is peaked around 1.0.

Charged pions generate hadronic showers in the EMC. However, the EMC cannot contain most of the shower energy. Therefore, E_{EMC}/p is dominant in the region below 0.8. Note the logarithmic ordinate in the plot for the pions.

Muons are minimum ionizing particles and therefore, deposit relatively little energy in the EMC. Their E_{EMC}/p distribution differs from the according distribution for pions, but an effective discrimination between muons and pions cannot be achieved by the use of E_{EMC}/p only. The muon-PID will be supplied by dedicated μ detectors in future versions of PandaRoot.

As a result, the E_{EMC}/p information can be used to distinguish between $e^\pm$ and $\pi^\pm$ if no muons are present or alternatively in combination with dedicated muon detectors. No intensive effort was put into optimizing the values on which a E_{EMC}/p cut needs to be applied, but the

following discrimination rules appear reasonable from the results obtained with the above method:

- If E_{EMC}/p falls within the interval between 0.8 and 1.2 and the muon detectors do not identify the particle as a muon, it is classified as an electron or positron depending on the charge determined from tracking.

- Particles which yield a value of E_{EMC}/p below 0.8 are classified as charged pions unless the muon detectors identify them as muons.

The effect of the aforementioned E_{EMC}/p cuts for electron and pion discrimination is demonstrated in a simulation of 5000 $\mathrm{p\overline{p}} \rightarrow \mathrm{X}(3872) \rightarrow J/\psi\ \pi^+\pi^- \rightarrow \mathrm{e^+e^-}\ \pi^+\pi^-$ events. The dedicated muon ID is unavailable in the utilized PandaRoot revision. As a compromise the decay $J/\psi \rightarrow \mu^+\mu^-$ is prohibited in EvtGen. The result for the two particle invariant mass of one electron candidate and one positron candidate is presented in figure 11: The background is reduced by about 90% in comparison with the previous case using no PID.

In section 6.3 the electron/ pion discrimination is applied to suppress inelastic hadronic backgroud from the DPM generator.

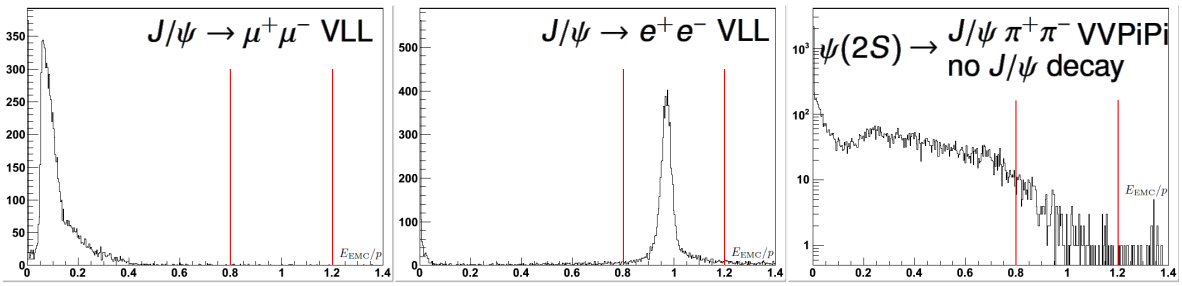

Figure 10: Plots of E_{EMC}/p for three different simulated decays are shown.

A simple electron/ pion discrimination can be achieved with a cut on the value of E_{EMC}/p. The muon-PID will have to be supplied by the dedicated μ detectors.

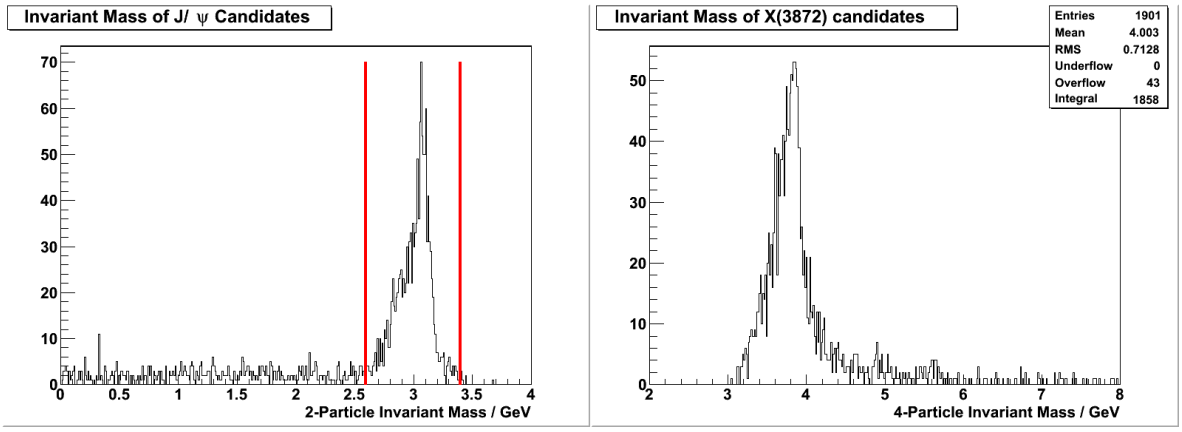

Figure 11: Plots of 5000 simulated $p\overline{p} \rightarrow X(3872) \rightarrow J/\psi\ \pi^+\pi^- \rightarrow e^+e^-\ \pi^+\pi^-$ are shown.

Left hand side: Invariant mass plot of two oppositely charged particles which satisfy the E_{EMC}/p condition demanded for $e^{\pm}$. The region for a cut on the J/ψ mass is indicated by two vertical red lines.

Right hand side: Four particle invariant mass spectrum for combinations of e^+e^- candidates which yield a J/ψ candidate within the J/ψ mass cut region and $\pi^+\pi^-$ candidates which were determined by the E_{EMC}/p PID cut only. A cut on the missing mass of the pions is not enforced here to demonstrate the effectiveness of the electron/ pion discrimination.

The plots shown in this figure correspond to the plots on the left hand side of figure 9. The difference is that here the aforementioned PID is applied and the four particle invariant mass is plotted for the J/ψ decay into electrons instead of muons.

6.3. Study of Inelastic Hadronic Background

As pointed out in section 5.3, a detailed simulation of inelastic hadronic background reactions in the center of mass energy region corresponding to the mass of the X(3872) is crucial to determine the feasibility of a resonance scan with $\overline{\mathrm{P}}$ANDA. Such events can be simulated using for instance the dual parton model (DPM) generator which is contained in PandaRoot.

In theory, the background simulation is easily done, but in practice, computing power and time constraints make it a hard problem. The compromise which is chosen in this thesis in order to obtain meaningful results under the given limitations is to simulate two different types of events:

- $2 \cdot 10^6$ inelastic hadronic background events are taken directly from DPM. These events are used to investigate the general background shape in the two and four particle invariant mass spectra.

- A second sample of $2 \cdot 10^6$ $\mathrm{p\overline{p}} \to \pi^+\pi^-\pi^+\pi^-$ events are analysed to determine the effect on a resonance scan of the X(3872). The events are produced by the DPM generator, but a filter is implemented and used in the DPM control program to reject all other types of reactions. In section 5.3 it is assumed that this process should dominate the background for a resonance scan of the X(3872) via the channel $J/\psi\,\pi^+\pi^-$ due to particle misidentification. These events also represent a good test for the $e^\pm/\pi^\pm$ discrimination implemented for this work (see section 6.2).

PandaRoot revision 11145 is used for the simulation and analysis of the aforementioned background events. The resulting two particle invariant mass spectra are presented in figure 12 for all inelastic hadronic events in the upper half and for $\mathrm{p\overline{p}} \to \pi^+\pi^-\pi^+\pi^-$ in the lower. For comparison, the left plots show the spectra without the electron/ pion discrimination and for the plots on the right hand side, this particular PID information is used. Out of $2 \cdot 10^6$ simulated background events for each of the aforementioned background types, only one event contained a possible J/ψ candidate in the invariant mass region close to the J/ψ mass. As expected, without PID the process $\mathrm{p\overline{p}} \to \pi^+\pi^-\pi^+\pi^-$ yields significantly more possible J/ψ candidates.

The corresponding four particle invariant mass spectra are presented in figure 13. The insets show that by applying the implemented electron/ pion discrimination in the analysis of the simulated background events, all fake X(3872) candidates are rejected. From $2 \cdot 10^6$ simulated background events for each of the aforementioned background types, not even one event contained a possible X(3872) candidate when the $e^\pm/\pi^\pm$ discrimination is combined with cuts on the invariant mass of $\mathrm{e^+e^-}$ candidates and on the missing mass of $\pi^+\pi^-$ candidates. The larger plots show the very same analysis, but without the application of the electron/ pion discrimination. For both background types the comparatively small signal of a resonance scan could not be detected without using the electron and charged pion PID.

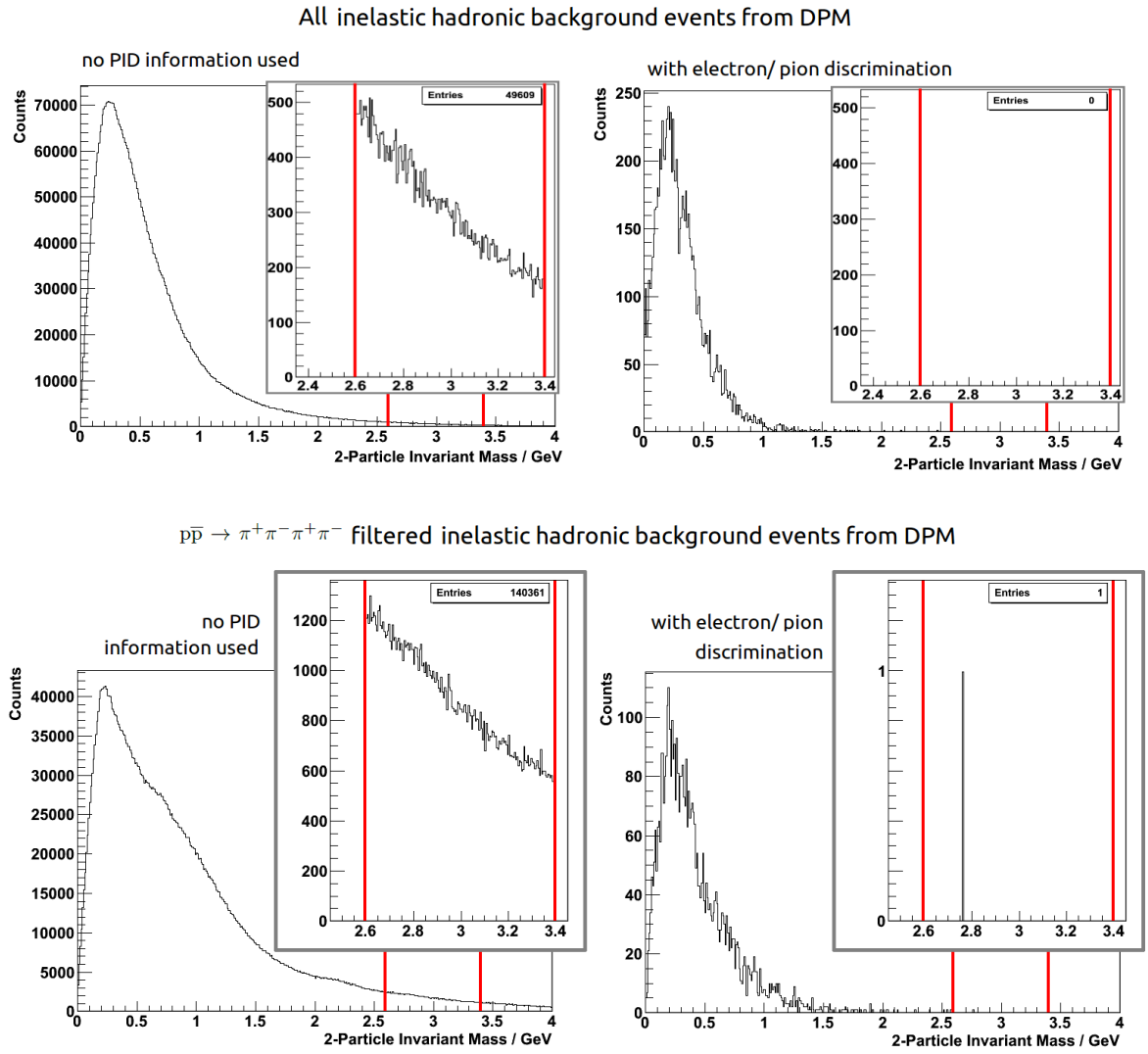

Figure 12: Invariant mass of two oppositely charged particles for 2 million inelastic hadronic background events (top) and 2 million processes $p\bar{p} \to \pi^+\pi^-\pi^+\pi^-$ (bottom). All events were produced using the DPM generator. The insets show the region on which an invariant mass cut for J/ψ candidates is applied for a reconstruction of X(3872) candidates.

For the left plots no particle identification information is used. The right plots show the result with the electron/ pion discrimination applied to the same Monte Carlo data sets.

As expected the process $p\overline{p} \to \pi^+\pi^-$ shows more J/ψ and X(3872) candidates in the crucial invariant mass regions. However, the electron/ pion discrimination works reliably enough to reject those background events.

The application of the electron/ pion discrimination to the background events gives a first indication that the feasibility of an X(3872) resonance scan with $\overline{\text{P}}$ANDA could be judged favourably, but it does not prove it. The computing time constraints did not allow for a full simulation of more background events. As mentioned before, the simulation was carried out on the cluster described in appendix D and in more detail in [44]. Resource consumption of other research projects as well as several harddisk crashes finally limited the possible number of processed background events for this thesis.

An estimate on the computing time needed for a complete background simulation can be obtained by the observation that the full simulation of 10^3 DPM background events with the TPC setup of the $\overline{\text{P}}$ANDA target spectrometer takes more than six hours on the utilized cluster using no parallelization. An optimistic assumption is that 100 jobs can be run in parallel. Further assuming no power outages and hardware failures, this leads to an estimated 8285 years[17] for the full simulation of the inelastic background from DPM for the whole resonance scan with 20 scan points of two days of data taking each. This amount of processing time is needed to simulate the full inelastic hadronic background for a complete resonance scan, but only for one detector setup. It is reasonable to assume that the background for all resonance scan points will be quite similar, therefore rendering it necessary to only simulate the background for one center of mass energy, for instance $E_{\text{cm}} = m_{\text{X(3872)}}$. Furthermore, it would be sufficient to have the simulation data for a good fraction of the total number of events and then to scale it up accordingly. Therefore, assuming it to be sufficient to simulate half an hour of inelastic background for one scan point, the required computing time is reduced to slightly more than 4.25 years for the inelastic hadronic background, but still prohibitive. Note that this estimate is obtained assuming no hardware failures, power outages and no use of the cluster for other research projects. Software optimization could possibly give some speed boost, but the most straightforward and effective approach is to employ more cores as the work load scales very well with the number of available cores. One option to consider is to run the backgroud simulation jobs on the $\overline{\text{P}}$ANDA grid. Another option to "improve" statistics at hardly any computing cost is to rotate the simulated data in φ and then just running the analysis on the rotated events. Apart from the the target pipes the target spectrometer is almost symmetric about the z-axis (see figure 3). This option could be considered if budgetary constraints dictate to do so. However, it is not a very compelling and convincing way to increase statistics.

[17] The estimated number of inelastic background events that occur per day when performing an X(3872) resonance scan is $3.024 \cdot 10^{10}$ (see equation (35) in section 5.3). For 2 days per scan point and a total of 20 scan points, the estimated number of inelastic background events is about $1.2 \cdot 10^{12}$. Assuming 100 jobs are executed in parallel and 10^3 jobs require a computing time of six hours leads to a theoretical total average cluster performance of $4 \cdot 10^5$ events per day. Almost 8285 years are needed to simulate all hadronic inelastic background events on the cluster which is equipped with up to date hardware (see appendix D). For the background from $p\overline{p} \to \pi^+\pi^-\pi^+\pi^-$, the result is significantly lower as $4.32 \cdot 10^7$ events are estimated according to equation (34) to occur per day of data taking at center of mass energies close to 3.872 GeV. Approximately 11.8 years are needed to simulate all background events of this type for the entire resonance scan.

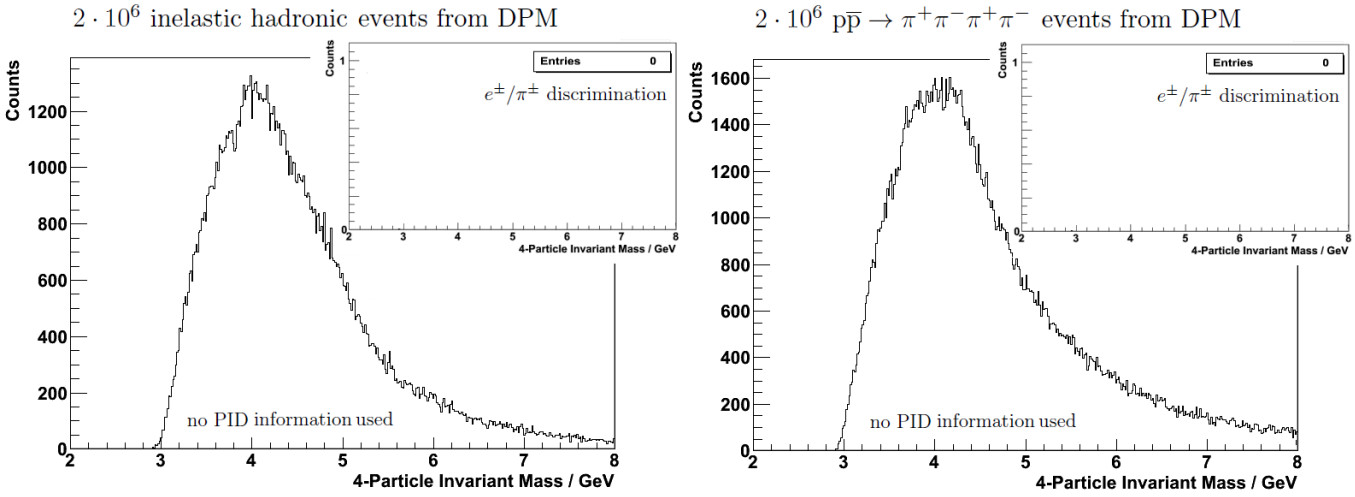

Figure 13: Invariant mass spectra of four oppositely charged particles for all inelastic hadronic events from the DPM generator (left hand side) and for $p\bar{p} \to \pi^+\pi^-\pi^+\pi^-$ filtered DPM events (right hand side). The larger plots show the distributions when no particle identification information is used. A large amount of possible X(3872) candidates is found in both types of background at masses around 3.872 GeV. The insets show the results when the electron/ pion discrimination is applied to the same Monte Carlo data sets.

For the reconstruction of the X(3872) candidates, a cut on the missing mass of the $\pi^+\pi^-$ candidates and a cut on the invariant mass of all e^+e^- candidates is enforced (as in section 6.1 and explained in more detail in section 6.4.2.).

For $\overline{\text{P}}$ANDA several possible detector options are discussed. The comparison of resonance scan results obtained for different detector layouts is especially hard to do as all background events essentially have to be rerun for every change in the detector setup. Different detector materials might lead to different interactions with primary or secondary particles. The computing power needed for a full background simulation considering one specific detector layout is already quite high as pointed out in the discussion above.

Future Monte Carlo simulations using more processor cores will have to follow in order to give a definite answer to the question what ratio of signal to inelastic hadronic background could be expected for a real resonance scan. The software developed for this thesis is designed and coded in a way that it can and will be utilized to produce and analyse large amounts of simulated background events in a highly automized and parallelized manner.

6.4. Simulation of a Resonance Scan of the X(3872) at $\overline{\text{P}}$ANDA

6.4.1. Technical Details of Resonance Scan Simulation

In order to simulate a resonance scan of X(3872) with the $\overline{\text{P}}$ANDA experiment, several currently unknown properties of X(3872) had to be assumed (see section 5.1). These estimates enter as parameters into the control script which was written for this thesis. Most notably, a mass $m_{\text{X(3872)}}$ of 3.872 GeV and a width $\Gamma_{\text{X(3872)}}$ of 100 keV are assumed. A full summary of the simulation parameters is provided in appendix A.

The X(3872) cross section is simulated according to the Breit-Wigner distribution for resonance formation in $\text{p}\overline{\text{p}}$ annihilations which is given in equation (20). The chosen X(3872) width is small enough to be treated as a constant. The antiproton beam momenta are assumed to be Gaussian distributed with standard deviations which correspond to HESR's high resolution mode. As a result, the corresponding center of mass energy distribution is also approximately Gaussian distributed (compare to section 4.2).

The excitation curve of X(3872) is investigated with a resonance scan of 20 energy scanpoints and a total of 40 days of simulated data taking. An accelerator duty factor of 50% is assumed and HESR's high resolution mode is chosen for the resonance scan. This will yield a luminosity of 864 nb^{-1} per day and a center of mass energy resolution of about 79 keV (FWHM) in the E_{cm} region of $m_{\text{X(3872)}}$ (see sections 5.1 and 4.2 for the calculations).

For the resonance scan simulation, a small energy shift of 10 keV between the closest scan point's energy and the true X(3872) mass is assumed. The reason is that it appears rather unrealistic that a real experiment would adjust the average beam momentum such that the center of mass energy matches exactly the maximum of the true X(3872) Breit-Wigner distributed cross section. Half the scan points are simulated at energies greater than the true $m_{\text{X(3872)}}$ and the other half is below this value. The energy scan points are chosen to range from 3871.540 MeV to 3872.490 MeV with equidistant spacings of 50 keV between them. This region was determined by exemplarily performing the numerical integration and calculating the resulting signal events that need to be simulated for an according scan point. The result is slightly above 5 events for subsequent J/ψ decays into e^+e^- only. Assuming that approximately half of these events will be reconstructed in the analysis, the result will be nearly consistent with 0 within the statistical error bars.

As the simulation does not use any dedicated muon detectors for particle identification, subsequent decays of $J/\psi \to \text{e}^+\text{e}^-$ are exclusively simulated. Decays into $\mu^+\mu^-$ are prohibited in EvtGen for the resonance scan's signal events in this work. Future versions of PandaRoot will supply dedicated muon PID and the J/ψ decay mode into $\mu^+\mu^-$ can be added for the resonance scan simulation. This will probably double or even triple the signal to backgroud ratio depending on the efficiency of the muon identification.

For every scan point which is defined by a nominal center of mass energy $E_{\text{cm},i}, i \in \{1, \ldots, 20\}$ the corresponding antiproton beam momentum $p_{\text{beam},i}$ is calculated according to equation 18.

For the determined value of $p_{\mathrm{beam},i}$, the standard deviation is calculated from the relative beam momentum uncertainty of $\Delta p_{\mathrm{beam},i}/p_{\mathrm{beam},i} \leq 2 \cdot 10^{-5}$ for HESR in high resolution mode. Using error propagation the according standard deviation $\Delta E_{\mathrm{cm},i}$ of the center of mass energy distribution is calculated (equation 26). The result differs slightly for every energy scan point and is used to model the center of mass energy distribution which is approximated by a Gaussian.

As pointed out in section 3.5, the effective cross section can be used to calculate the number of signal events that need to be simulated for a given scan point. In order to obtain the effective cross section, the integral in equation (23) is solved numerically using a comparison of several one dimensional numerical integration methods which are implemented in root[18]. The integration intervals are varied over several orders of magnitudes in terms of standard deviations of the approximated Gaussian distribution. As the individual methods show different weaknesses which lead to nearly random results when the integration interval is not set properly, the most frequent result of all integrations is selected as the most reasonable result.

The effective cross section which is obtained from numerical integration can be used to calculate the number of signal events that need to be simulated by multiplying with the integrated luminosity of 0.864 pb^{-1} per day (see equation 22 and section 5.1). The result is the number of X(3872) formed in $\mathrm{p\overline{p}}$ collisions per day. Multiplying with the assumed branching ratio for X(3872) $\rightarrow J/\psi\ \pi^+\pi^-$ which was chosen to be 0.1 and then with the branching ratio of $J/\psi \rightarrow \mathrm{e^+e^-}$ ($\approx 6\%$ [1]) gives the number of signal events to simulate for the according resonance scan point. Multiplying this intermediate result with the number of 2 days per scanpoint yields the final number of events to be simulated for the scanpoint. All these calculations are performed automatically in the PandaRoot macro which is responsible for the event generation with EvtGen and particle transport using Geant 3.

The number of background events from the direct $\mathrm{p\overline{p}} \rightarrow J/\psi\ \pi^+\pi^-$ process is assumed to be constant for all scan points. In [2] the cross section for this process is estimated to be approximately 1.2 nb and to remain nearly constant over the center of mass energy range of interest. Multiplying this cross section with the integrated luminosity of 0.864 pb^{-1} per day, with the number of days per scanpoint and with $\mathrm{BR}(J/\psi \rightarrow \mathrm{e^+e^-}) \simeq 0.06$ yields the number of background events that need to be simulated for each scan point. The result of 124.416 is rounded to 124.

In the simulation of the resonance scan, this background is simulated separately from the signal events and the background simulation processes are initialized with different random seeds. The background events are analyzed with the same macros as the signal. Signal and background events are added for the result of the simulated resonance scan. The applied

[18] ROOT::Math::IntegrationOneDim::kADAPTIVE is suitable for general functions without singularities and gives reliable results over wide ranges of integration intervals. For comparison ROOT::Math::IntegrationOneDim::kADAPTIVESINGULAR (adaptive integration method which can be used in case singularities are present), ROOT::Math::IntegrationOneDim::kGAUSS (Gauß integration method) and ROOT::Math::IntegrationOneDim::kNONADAPTIVE (intended for smooth functions) are used. The latter give reasonable results for limited ranges of integration intervals. By comparing results obtained from different methods and various integration intervals, the most reasonable result can be chosen.

fit has no information about how many counts originate from background processes or from signal events.

The fit routine is written in root. It uses the following macros as a basis and combines them with self written functions for the Gaussian distribution given in equation (12) and the Breit-Wigner distribution from equation (20):

$ROOTSYS/tutorials/fit/langaus.C: This macro uses a routine to fit a convolution of Landau and Gaussian distributions to data.

$ROOTSYS/tutorials/fit/FittingDemo.C: This macro is an example illustrating how to fit signal and background.

The parameters used to fit the line shape of the resonance scan are a constant for the background from $p\overline{p} \to J/\psi\ \pi^+\pi^-$, the mass $m_{\mathrm{X(3872)}}$ of the X(3872), its width $\Gamma_{\mathrm{X(3872)}}$, and the product of its branching ratios $\mathrm{BR(X(3872)} \to p\overline{p}) \cdot \mathrm{BR(X(3872)} \to J/\psi\ \pi^+\pi^-)$ as well as the standard deviation of the Gaussian and a parameter for the integral of the convolution of Gaussian and Breit-Wigner. All parameters were allowed to be varied over several orders of magnitude and the starting values were chosen to be close to, but reasonably distant from the true values. It should be noted that the standard deviation of the according Gaussian is not known as it is not necessarily identical to the Gaussian center of mass energy distribution. The entire simulation of the X(3872) resonance scan with $\overline{\text{P}}$ANDA was performed within PandaRoot revision 12107. Signal and background events were created directly within PandaRoot using the EvtGenDirect interface to EvtGen. Geant3 was used as transport engine. The utilized detector setup code can be found in appendix B.

In later versions of PandaRoot that will feature dedicated muon identification, the J/ψ reconstruction from $\mu^+\mu^-$ can be added. The branching ratio for $J/\psi \to \mu^+\mu^-$ is about 6% [1]. The same branching ratio as for $J/\psi \to e^+e^-$. Therefore, by adding the $\mu^+\mu^-$ decay channel, the number of signal events will be doubled for otherwise identical simulation parameters. Also the number of background events needs to be doubled. However, the result should be easier to fit and not as susceptible to random fluctuations as the simulated data obtained using the $J/\psi \to e^+e^-$ decay only.

6.4.2. Reconstruction Procedure

As a first step, the electron/ pion discrimination developed in section 6.2 is applied to classify all charged particles present in the events into $e^{\pm}$ and $\pi^{\pm}$ candidates. All combinations of one electron and one positron candidate in the same event are used to calculate the two particle invariant mass. If the result falls within the J/ψ mass region from 2.6 GeV to 3.4 GeV, this combination is regarded as a J/ψ candidate.

For all $\pi^+\pi^-$ candidates from the same event, the missing mass is calculated. The result also has to be in the J/ψ mass region from 2.7 GeV to 3.5 GeV for the event to be further analysed. Note that for the missing mass the boundaries are chosen to be 100 keV greater than for the invariant mass of the e^+e^- pair. This takes energy loss of electrons and positrons due to final state radiation into account.

If the event contains one or more suitable J/ψ candidates and at least one possible $\pi^+\pi^-$ pair with a missing mass in the correct region, the according four particle invariant mass is calculated. If the result falls within the interval from 3.6 GeV to 4.0 GeV, the X(3872) candidate counter for the scanpoint is raised by one. Figure 15 shows the results of the signal simulation for each resonance scan point.

This analysis method is used in the same way for the X(3872) signal ($p\overline{p} \rightarrow$ X(3872) $\rightarrow J/\psi\ \pi^+\pi^- \rightarrow e^+e^-\pi^+\pi^-$) as well as for the background from $p\overline{p} \rightarrow J/\psi\ \pi^+\pi^- \rightarrow e^+e^-\pi^+\pi^-$. The according X(3872) candidates are presented in figure 15 for the simulated signal events and in 16 for the according background events.

The X(3872) candidate counts from the background and the signal are added for each point of the resonance scan. The results are shown in figure 14. The fit which is then applied has no information about how many counts are due to background processes or how many originate from signal events.

6.4.3. Results from Resonance Scan Simulation

The lineshape obtained from the simulation of an X(3872) resonance scan with $\overline{\text{P}}$ANDA as described in section 6.4.1 is presented in figure 14. The nominal center of mass energy corresponds to the horizontal axis. The vertical axis of the excitation curve corresponds to the counts of reconstructed X(3872) candidates at the respective scan point. The reconstruction method for X(3872) candidates used to obtain the counts in figure 14 is outlined in section 6.4.2.

The simulated results are fitted with a convolution of a Gaussian (see equation (12)) and a Breit-Wigner distribution (see equation (20)) plus a constant for the direct X(3872) $\rightarrow$ $J/\psi\ \pi^+\pi^-$ background. The fit is only used to estimate the full width at half maximum W_{obs} of the observed excitation function. This value allows to estimate the width of the X(3872). As described in [3], the width $\Gamma_{\text{X(3872)}}$ of the underlying Breit-Wigner distribution can be estimated with a maximum systematic error of 4% if the full width at half maximum W_{G} of the Gaussian error distribution is known exactly using the following equation:

$$\Gamma_{\text{X(3872)}} \simeq W_{\text{obs}} - \frac{(1.02 \cdot W_{\text{G}})^2}{W_{\text{obs}}} \tag{36}$$

As an approximation, the FWHM of the center of mass energy distribution estimated in section 4.2 is assumed for W_{G}. Setting W_{G} to 79 keV and obtaining $W_{\text{obs}} \approx 152.6$ keV from the fit in figure 14 yields the following estimate on $\Gamma_{\text{X(3872)}}$:

$$\Gamma_{\text{X(3872)}} \approx 152.6\ \text{keV} - \frac{(1.02 \cdot 79\ \text{keV})^2}{152.6\ \text{keV}} \approx 110.0\ \text{keV}. \tag{37}$$

This straightforward procedure yields an acceptable result for the width of the X(3872) which is about 10% greater than the input width of 100 keV. The error of this estimate should be dominated by the estimation of W_{G} and the statistical fluctuations of the observed signal counts and not by using the above approximation.

It should be noted that having dedicated muon detectors available in future PandaRoot revisions will improve the statistics significanly and especially the count fluctuations of the background events can be expected to be less prominent than for this simulation which allowed J/ψ decays to e^+e^- only. The fluctuations of counts from background events can be estimated from the X(3872) candidates presented in figure 16.

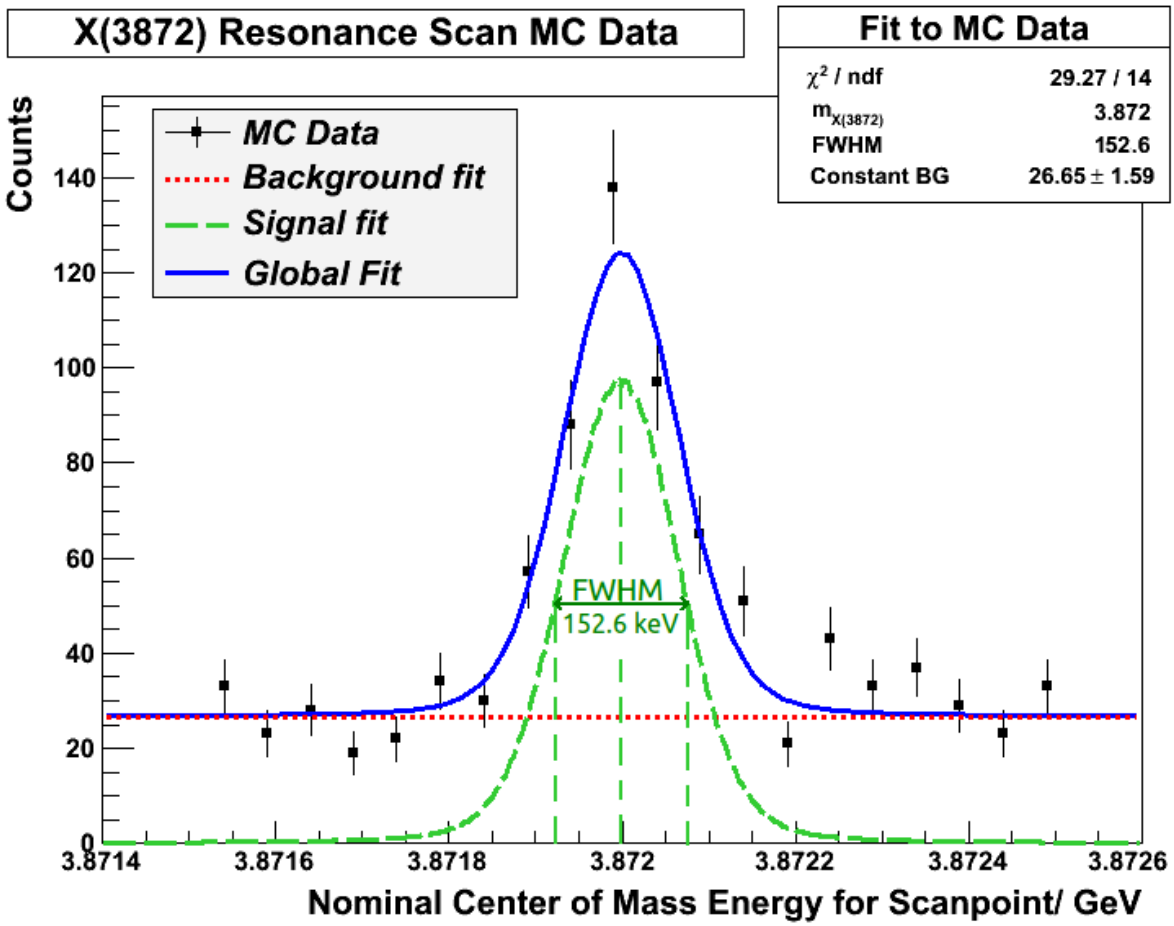

Figure 14: Result for the simulated resonance scan of X(3872) with 20 equidistant center of mass energy scan points. The process $p\bar{p} \rightarrow$ X(3872) $\rightarrow J/\psi\ \pi^+\pi^-$ VVPiPi with subsequent $J/\psi \rightarrow e^+e^-$ VLL decay was simulated within the PandaRoot framework. Direct background from $p\bar{p} \rightarrow J/\psi\ \pi^+\pi^-$ is taken into account. The simulation parameters are summarized in table 4 (appendix A).

Electron/ pion discrimination is used for particle identification. The center of mass energy distribution is approximated by a Gaussian. The according standard deviation is calculated for each energy scan point according to the beam momentum spread for HESR in high resolution mode.

The fit to the simulated signal including background is performed with a convolution of a Gaussian – representing the center of mass energy spread and detector inaccuracies – and a Breit- Wigner distribution – describing the X(3872) cross section – plus a constant – taking the background from the direct $J/\psi\ \pi^+\pi^-$ production into account. The fit is used to estimate the FWHM of the observed distribution. $\Gamma_{X(3872)}$ is calculated according to equation (36). The obtained result is 110.0 keV, i.e. about 10% larger than the input width. Only statistical errors are shown.

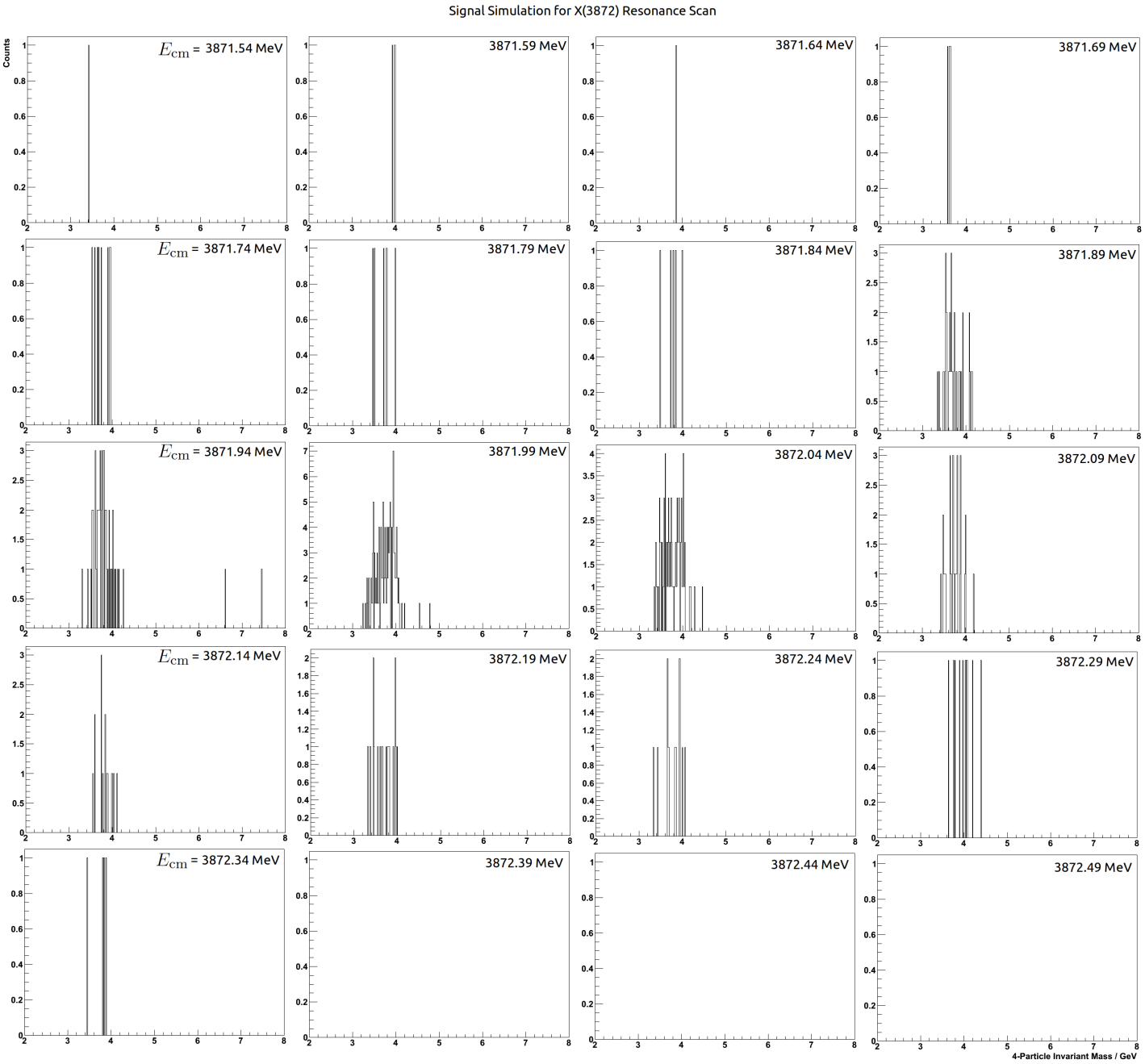

Figure 15: For every simulated resonance scan point, the four particle invariant mass spectrum from signal simulation is plotted. The nominal center of mass energy for each scan point is presented in the upper right corner of each subplot. The X(3872) candidates are determined as described in section 6.4.2. Only candidates with a mass in the region of 3.872 GeV from 3.6 GeV to 4 GeV are counted. The according X(3872) candidate count for the background simulations shown in figure 16 are added for each scan point. Figure 14 shows the result.

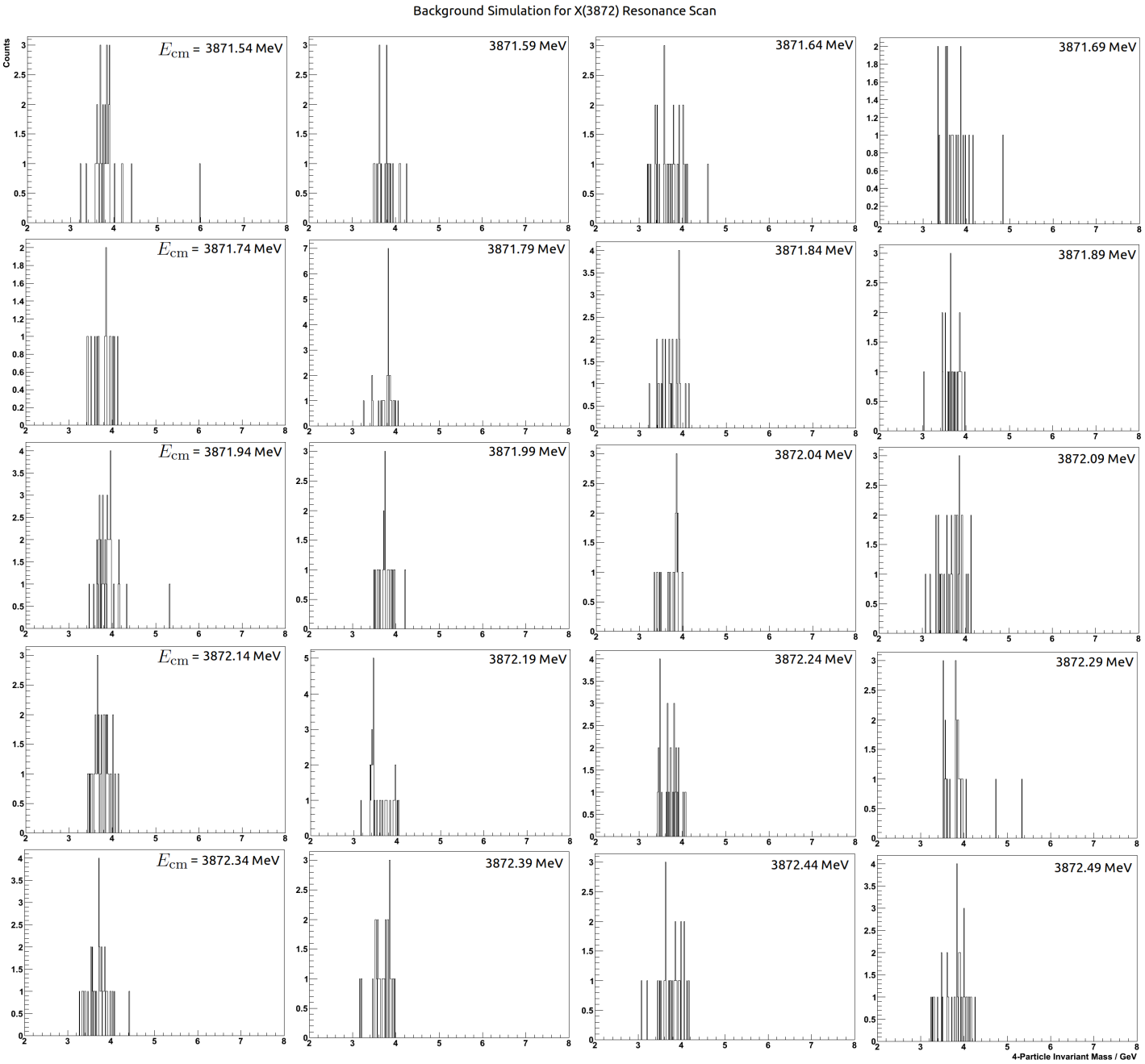

Figure 16: For every simulated resonance scan point, the four particle invariant mass spectrum from $p\bar{p} \to J/\psi\ \pi^+\pi^-$ background simulation is plotted. The nominal center of mass energy for each scan point is presented in the upper right corner of each subplot. The X(3872) candidates are determined as described in section 6.4.2. Only candidates with a mass in the region of 3.872 GeV from 3.6 GeV to 4 GeV are counted. The according X(3872) candidate count for the signal simulations shown in figure 15 are added for each scan point. Figure 14 shows the result.

7. Conclusions and Outlook

7.1. Scientific Results

The cut on E_{EMC}/p developed in this thesis has been successfully used to reject inelastic hadronic background both directly from the DPM generator as well as filtered events which only contained $\pi^+\pi^-\pi^+\pi^-$ for the final state of interest in this work. The process $\mathrm{p\overline{p}} \to \pi^+\pi^-\pi^+\pi^-$ was assumed to be the dominant source of background due to possible charged pion misidentification. From $2{\cdot}10^6$ simulated background events for each of the aforementioned background types, not one event contained a possible X(3872) candidate. This is a good sign for the feasibility of an X(3872) resonance scan with $\overline{\mathsf{P}}\mathsf{ANDA}$. However, future Monte Carlo simulations using more processor cores will have to follow in order to give a definite answer to the question what ratio of signal to inelastic hadronic background could be expected for a real resonance scan. The software developed for this thesis can be helpful to produce and analyse large amounts of simulated background events in a highly automized manner.

A detailed resonance scan of the X(3872) was simulated entirely in PandaRoot using preexisting macros which were adjusted and new bash scripts which were written for this work. 20 energy scan points of two days datataking each were assumed. The background from $\mathrm{p\overline{p}} \to \pi^+\pi^-\pi^+\pi^-$ was taken into account and the resonance cross section was implemented as a Breit-Wigner distribution. The center of mass energy distribution was approximated by a Gaussian.

By fitting a convolution of a Breit-Wigner and a Gaussian to the obtained line shape, the full width at half maximum of the observed distribution was estimated. This result allowed to estimate the width of the X(3872) according to equation (36). The result of $\Gamma_{\mathrm{X(3872)}} \approx 110.0$ keV was found to be 10% greater than the input width 100 keV. This straightforward procedure yields an acceptable result for $\Gamma_{\mathrm{X(3872)}}$ even though random fluctuations are rather prominent in the simulated signal counts. The availability of dedicated muon detectors will improve the statistics significanly and fluctuations can be expected to have a smaller impact than in this simulation which only allowed J/ψ decays to $\mathrm{e^+e^-}$.

The simulation assumed a very narrow width for the X(3872) and a relatively small production cross section of 50 nb in $\mathrm{p\overline{p}}$ annihilations. Therefore, the simulation performed in this work can be regarded as a worst case scenario (assuming inelastic hadronic background has a negligible effect on the outcome and feasibility of the simulated resonance scan). If the model calculations in [2] are correct, either the true X(3872) width should be significantly larger for the cross section assumed in this work or in case the true width $\Gamma_{\mathrm{X(3872)}}$ is close to the assumed value, the total cross section should be significantly larger than the chosen value of 50 nb.

In order to use advanced unfolding methods [45, 46] such as singular value decomposition [47] for an analysis carried out on real data, a detector response matrix for $\overline{\mathsf{P}}\mathsf{ANDA}$ needs to be obtained using a large amount of simulated Monte Carlo events. The software written for this work is designed to produce and analyse such MC simulated events.

7.2. Technical Aspects

As discussed in section 2, the PandaRoot framework is still under development and the final detector layout for $\overline{\mathsf{P}}$ANDA has not been decided on. Therefore, the software needs to be flexible. Considering that manpower is limited, the software which is needed to perform a resonance scan should allow for frequent reusability requiring little human attention.

The development of a highly automated computational base was aimed at and achieved in this work: The user sets the environment for the desired version of PandaRoot, chooses what type of simulation[19] and detector layout[20] is wanted by adjusting predefined parameters in a central control script named *batch.sh*, then navigates to it in the shell bash and calls the script by typing *". batch.sh"*. The script takes care of splitting the workload into small parts and automatically submits the jobs to the resource manager. This method takes advantage of today's and future multi-core computer systems and batch farms. It required some adjustments of the PandaRoot macros which were deployed previously.

The user then waits for the job to finish. All data handling is taken care of by a second control script called *sim.sh* which does not require any interaction with the user, but can also be called directly for debugging purposes. After the processing of some or all simulation files, the user can check the data integrity and the progress of the jobs by calling a script named *progresscheck.sh* which can automatically delete corrupt data and resubmit the according jobs to be reprocessed by the batch farm if the user wishes to do so. This represents the typical behavior for mass production of background events. For debugging, the script can be advised to point out which jobs have probably failed and gives hints what possible reasons are. During the production of background events for this thesis, several hardware failures such as crashing hard disk drives and possibly overheating CPUs or general operating system and batch farm software hang-ups have resulted in different errors can be detected by the script.

The final results are obtained using the user's analysis PandaRoot macro. An advantage of the aforementioned automatization is that the user can focus mainly on his or her analysis macro and does not need to be knowledgable in Monte Carlo simulations.

The aforementioned tools are suitable to be used as a basis for resonance scan simulations of other X(3872) decay channels or other particles of interest. The software developed in this work is already successfully applied to a study of $\mathrm{p\overline{p}} \to \mathrm{X}(3872) \to J/\psi\ \gamma$ in [48].

Another possible use of the software written for this thesis is to compare various possible detector layouts. The scripts and macros are already capable to switch between the discussed

[19] Several X(3872), $\Psi(2S)$, J/ψ signal decays are supported, other options include: Simulation of DPM background using directly the DPM output or reading in files that contain filtered DPM output – for instance only $\pi^+\pi^-\pi^+\pi^-$ events – and signal decays for a resonance scan. The resonance mass, width, branching ratios and cross section are parameters that can easily be adjusted in the cental control script. The number of equidistant scan points, the days for each scan point and the shift between the maximum of the Breit-Wigner distribution and the closest central scan point can be adjusted as well. The HESR mode can be switched between high resolution and high luminosity.

[20] Currently STT and TPC layouts are supported in the scripts and macros. Further options can be included as outlined in appendix C. Geant3 or Geant4 can be used for particle transport.

STT and TPC layouts for the $\overline{\mathsf{P}}$ANDA target spectrometer. $2 \cdot 10^6$ background DPM events with a filter on $p\bar{p} \to \pi^+\pi^-\pi^+\pi^-$ were simulated both for the TPC and the STT layout in preparation of a comparison of these two options. Unfortunately, the PandaRoot development version from Mid- March 2011 (revision 11145) which was used for the simulation does not support the STT setup and therefore, only the TPC results can be presented in this work. A comparison using a future version of PandaRoot can easily be done in terms of required manpower, but note that a *realistic* assessment of the influence of various detector layouts requires a large number of backgroud events to be resimulated for every detector layout under investigation – which takes a lot of computing time (see the discussion in section 6.3).

Closely related to the previous paragraph is the following point: In future studies more background events need to be simulated in order to be able to estimate the expected background suppression of the detector for a real X(3872) resonance scan. The feasibility of such an endeavor will strongly depend on this information. With a soon to be released up-to-date stable production version of PandaRoot which will feature numerous improvements, a production of a large amount of background events for the X(3872) resonance scan is planned. The software set developed in this work will be very helpful for this project.

Comparatively easy to achieve with the tools from this thesis in terms of required manpower and computing time is the resonance scan simulation for a given detector layout assuming various widths $\Gamma_{\mathrm{X(3872)}}$. Only one parameter needs to be changed in the central control script *batch.sh*. The time-consuming simulatino of inelastic hadronic background events does not have to be repeated when only the width of the resonance is changed. Note that for larger X(3872) widths, $\Gamma_{\mathrm{X(3872)}}$ should not be treated as a constant as pointed out in section 3.5. The software can be adjusted to account for that. The resonance scan can easily be adapted for non-equidistant scanpoints if necessary. The number of days per scanpoint can be made non-uniform. Additional possible improvements include the implementation of kinematic fits to compensate for final state radiation and adding a decay model to EvtGen which describes the decay of a 1^+ particle into $J/\psi\ \pi^+\pi^-$ more accurately than the utilized VVPiPi.

Future iterations of the PandaRoot framework need to offer more sophisticated particle identification to its users. Especially the implementation of the muon detectors is important for the resonance scan simulation in this work. Including the channel $\mathrm{X(3872)} \to J/\psi\ \mu^+\mu^-$ could double or even triple the signal counts depending on the efficiency of the muon detection. In case the background suppression is equally good or better than the electron pion discrimination implemented in this work, the signal to backgroud ratio could be significantly improved. The E_{EMC}/p based electron pion discrimination can be used as a basis for a more sophisticated particle identification taking more subdetectors into account which could improve the efficiency for the observed channels.

As in section 2.4.4 of [27] the center of mass energy distribution was assumed to be Gaussian. However, for future Monte Carlo resonance scan simulations it would be advantageous to incorporate a more detailed beam spread into PandaRoot, for instance as described in [32] where the beam momentum spread is calculated from the beam revolution frequency distribution which is approximated by a double Gaussian. A double Gaussian is comprised of two half Gaussians joined together at their maximum points. For the E-760 experiment, the low energy half is about 10% to 20% wider than the high energy part. The beam momentum

spread can be calculated from the revolution frequency distribution and implies an according center of mass distribution. The authors also consider possible correction terms in form of exponential tails or polynomials which they find have negligible effects on the physics results obtained from the resonance scan carried out in their experiment.

Further studies could consider the effects that arise due to initial state radiation of the $p\overline{p}$ system. In [32] the widths $\Gamma_{J/\psi}$ and $\Gamma_{\psi'}$ were determined with a resonance scan. The authors state that the width for J/ψ is decreased by approximately 10 keV and for the ψ', initial state radiation is found to affect the width determination only by 2 keV. The mass measurements were ascertained to not be affected. It can be assumed that the effects on the X(3872) will be equally small and therefore, bremsstrahlung of initial $p\overline{p}$ state was neglected in this work.

Once the final detector setup is known and completely implemented in PandaRoot the use of more sophisticated unfolding procedures [45, 46] can be prepared. Unfolding algorithms such as the singular value decomposition (SVD) [47] need a Monte Carlo input which can be conveniently obtained using the scripts and macros developed in this work.

The software developed in this thesis will be very helpful for future work and can easily be adapted to related fields of study and advanced to take additional physical details into account as described above. It works completely within PandaRoot and the UNIX shell bash and does only require physical parameters such as the mass, width, cross section and branching ratios for the resonance under investigation as an input. The parameters can be adjusted in a central script. The resonance scan simulation does not require any externally calculated numbers for event generation. The numerical integration is carried out in PandaRoot. In case of hardware failures or power outages, the script *progresscheck.sh* can be used to detect corrupted data which can automatically be deleted and then be resubmitted for recomputation. The software is easy and convenient to use and it significantly reduces the manpower and time required to perform simulated resonance scans which will have to be carried out repeatedly for future versions of PandaRoot. The effectiveness of the software is proven by presenting new results from a resonance scan simulation of the X(3872).

References

[1] K. Nakamura et al. (Particle Data Group):
J. Phys. G37, 075021 (2010)

[2] G. Y. Chen, J. P. Ma:
Production of X(3872) at $\overline{\text{P}}$ANDA
Phys. Rev. D77 097501 (2008)

[3] J. G. McEwen, G. J. Daniell:
A Note on Determining Resonance Widths in the Presence of Gaussian Errors
Nuclear Instruments and Methods 116 (1974)

[4] S. L. Glashow, J. Iliopoulos, L. Maiani:
Weak Interactions with Lepton-Hadron Symmetry
Phys. Rev. D 2, 1285-1292 (1970)

[5] U. Ellwanger:
Vom Universum zu den Elementarteilchen –
Eine erste Einführung in die Kosmologie und die fundamentalen Wechselwirkungen
Springer (2008)

[6] $\overline{\text{P}}$ANDA Collaboration:
Technical Design Report for the $\overline{\text{P}}$ANDA Solenoid and Dipole Spectrometer Magnets
arXiv:0907.0169v1 [physics.ins-det] (2009)

[7] S. Eidelman et al. (Particle Data Group):
Phys. Lett. B592, 1 (2004).

[8] K. Königsmann:
Open Problems in Charmonium Spectroscopy
SuperLEAR Workshop, Zurich, Switzerland, 9 - 12 Oct 1991, pp.71-84

[9] M. Werner:
Search for new bottomonium(-like) states in $e^+e^- \to B^{(*)}\bar{B}^{(*)}(\pi)(\pi)$ at the BELLE experiment
Master Thesis (2010)

[10] S.-K. Choi, S.L. Olsen, et al. (Belle Collaboration):
Observation of a narrow charmonium-like state in exclusive $B^+ \to K^+\pi^+\pi^- \; J/\psi$ decays
Phys. Rev. Lett. 91 262001 (2003)

[11] B.Aubert, et al. (BaBar Collaboration):
Study of the $B^- \to J/\psi K^-\pi^+\pi^-$ Decay and Measurement of the $B^- \to$ X(3872)K^- Branching Fraction
Phys. Rev. D71 071103 (2005)

[12] D. Acosta et al. (CDF II Collaboration):
Observation of the Narrow State X(3872) $\to J/\psi \; \pi^+\pi^-$ in $\overline{\text{p}}$ p Collisions at $\sqrt{s} =$ 1.96 TeV
Phys. Rev. Lett. 93 072001 (2004)

[13] V. M. Abazov et al. (D0 Collaboration):
Observation and Properties of the X(3872) Decaying to $J/\psi\ \pi^+\pi^-$ in p $\overline{\text{p}}$ Collisions at $\sqrt{s} = 1.96$ TeV
Phys. Rev. Lett. 93 162002 (2004)

[14] The LHCb Collaboration:
Measurement of the X(3872) mass with first LHCb data
LHCb-ANA-2011-030 (2011)

[15] A. Abulencia, et al. (CDF Collaboration):
Analysis of the Quantum Numbers J^{PC} of the X(3872) Particle
Phys. Rev. Lett. 98, 132002 (2007)

[16] K. Abe, et al. (Belle Collaboration):
Experimental constraints on the possible J^{PC} quantum numbers of the X(3872)
arXiv:0505038v1 [hep-ex] (2005)

[17] P. del Amo Sanchez, et al. (Babar Collaboration):
Evidence for the decay X(3872) $\rightarrow J/\psi\ \omega$
Phys. Rev. D82, 011101 (2010)

[18] P. Colangelo, et al.:
$X(3872) \rightarrow D\bar{D}\gamma$ decays and the structure of X(3872)
Phys. Lett. B650 166 (2007)

[19] J.L. Rosner:
Effects of S-wave thresholds
Phys. Rev. D74 076006 (2006).

[20] D.V. Bugg:
Reinterpreting several narrow 'resonances' as threshold cusps
Phys. Lett. B598 8 (2004)

[21] L. Maiani, F. Piccinini, A.D. Polosa and V. Riquer:
Diquark-antidiquark states with hidden or open charm and the nature of X(3872)
Phys. Rev. D71 014028 (2005)

[22] B.A. Li:
Is X(3872) a possible candidate of hybrid meson
Phys. Lett. B605 306 (2005)

[23] D. Ebert, R.N. Faustov and V.O. Galkin:
Masses of heavy tetraquarks in the relativistic quark model
Phys. Lett. B634 214 (2006)

[24] E. Braaten and M. Kusunoki:
Exclusive production of the X(3872) in B meson decay
Phys. Rev. D71, 074005 (2005).

[25] `http://www.adaptivecomputing.com/resources/docs/torque/`

[26] `http://www.adaptivecomputing.com/resources/docs/maui/mauiadmin.php`

[27] $\overline{\text{P}}$ANDA Collaboration:
Physics Performance Report for $\overline{\text{P}}$ANDA: Strong Interaction Studies with Antiprotons
arXiv:0903.3905 [hep-ex] (2009)

[28] FAIR Project:
Baseline Technical Report
Technical report, GSI, Darmstadt, (2006)

[29] B. Gålnander:
Status of Electron Cooler Design for HESR
Proceedings of EPAC08, Genoa, Italy, THPP049, page 3473 (2008)

[30] H. Stockhorst et al:
Stochastic Cooling Developments for the HESR at FAIR
Proceedings of EPAC08, Genoa, Italy, THP055, page 3491 (2008)

[31] A. Lundborg, T. Barnes and U. Wiedner:
Charmonium Production in $p\overline{p}$ annihilation: Estimating Cross Sections from Decay Widths
Phys. Rev. D73 096003 (2006)

[32] T. A. Armstrong, D.Bettoni, et. al (E760 Collaboration):
Measurement of the J/ψ and ψ' resonance parameters in $p\overline{p}$ annihilation
Phys. Rev. D 47 772–783 (1993)

[33] `http://panda-wiki.gsi.de/cgi-bin/view/Computing/PandaRoot`

[34] R. Brun and F. Rademakers:
ROOT – An object oriented data analysis framework
Phys. Res. A389, 81-86 (1997)

[35] S. Spataro:
Simulation and event reconstruction inside the PandaRoot framework
Journal of Physics 119 032035 (2008)

[36] M. N. Wagner:
Suche nach Charmoniumzuständen mit Proton-Antiproton Endzuständen im Rahmen des Belle-Experimentes
Bachelor Thesis (2010)

[37] V. Uzhinsky, A. Galoyan:
Cross Sections of Various Processes in Pbar P-Interactions
arXiv:hep-ph/0212369 (2002)

[38] V. Flaminio et al.:
Compilation of Cross-Sections, Part 3, p and anti-p Induced Reactions
High-Energy Reactions Analysis Group, CERN-HERA-79-03 (1979)

[39] D. J. Lange:
The EvtGen particle decay simulation package
Nucl. Instrum. Meth. A462, 152 - 155 (2001)

[40] E. Barberio, B. van Eijk, Z. Was:
Photos – a universal Monte Carlo for QED radiative corrections in decays
Comp. Phys. Comm. 66 115 (1991)

[41] R. Brun et al.:
CERN DD/EE/84-1 (1987)

[42] R. Brun et al.:
CERN Program Library Long Writeup W5013 (1994)

[43] S. Agostinelli et al.:
GEANT4: A simulation toolkit
Nucl. Instrum. Meth. A506, 250 (2003).

[44] M. J. Galuska, T. Geßler:
The Computing Cluster
Study Project (2010)

[45] V. Blobel:
Unfolding – Linear Inverse Problems
Notes for the Terrascale workshop at DESY May 2010

[46] T. Adye:
Unfolding algorithms and tests using RooUnfold
arXiv:1105.1160v1 [physics.data-an] (2011)

[47] A. Höcker:
SVD Approach to Data Unfolding
arXiv:9509307v2 [hep-ph] (1995)

[48] S. A. Braun:
Monte-Carlo Simulation für den Zerfall X(3872) $\rightarrow J/\psi\ \gamma$ am $\overline{\text{P}}$ANDA Experiment
(Working Title)
Bachelor Thesis (2011)

[49] T. J. Burns:
Rethinking the X(3872)
arXiv:1101.4816v1 [hep-ph] (2011)

[50] J. S. Lange, M. J. Galuska, et al.:
Prospects for X(3872) Detection at $\overline{\text{P}}$ANDA
arXiv:1010.2350v2 [hep-ex] (2010)

[51] J. S. Lange for the $\overline{\text{P}}$ANDA Collaboration:
The $\overline{\text{P}}$ANDA Experiment – Hadron Physics with Antiprotons at FAIR
International Journal of Modern Physics A, Vol. 24, Nos. 2-3 pp. 369-376 (2009)

[52] N. Brambilla et al.:
Heavy quarkonium: progress, puzzles, and opportunities
arXiv:1010.5827v3 [hep-ph] (2010)

[53] M. Andreotti et. al (Fermilab E835 Collaboration):
Precision measurements of the total and partial widths of the ψ' charmonium meson with a new complementary-scan technique in $\overline{\mathrm{p}}$ p annihilations
Phys. Lett. B 654 74-79 (2007)

[54] D. C. Kennedy:
Bremsstrahlung for p$\overline{\mathrm{p}}$ production of charmonium
Phys. Rev. D 46 461–462 (1992)

[55] B. Povh, K. Rith, C. Scholz, F. Zetsche:
Teilchen und Kerne – Eine Einführung in die physikalischen Konzepte
7. Aufl. Springer (2006)

[56] J. M. Blatt, V. F. Weisskopf:
Theoretical Nuclear Physics
John Wiley & Sons, Inc. (1966)

[57] C. Berger:
Elementarteilchenphysik –
Von den Grundlagen zu den modernen Experimenten
2. Aufl. Springer (2006)

[58] F. Hinterberger:
Physik der Teilchenbeschleuniger und Ionenoptik
2. Aufl. Springer (2008)

[59] M. C. Mertens:
Der $\overline{\mathsf{P}}$ANDA Mikro Vertex Detektor:
Entwicklung eines Labormesssystems, Simulation der MVD-Betriebsparameter sowie Untersuchungen zur Auflösung der Breite des $D^*_{s0}(2317)$
PhD Thesis (2010)

[60] M. J. Galuska:
Suche nach dem $\eta_\mathfrak{b}$ in den Zerfällen: $\boldsymbol{\Upsilon}(\mathbf{3S})$, $\boldsymbol{\Upsilon}(\mathbf{4S})$, $\boldsymbol{\Upsilon}(\mathbf{5S}) \to \eta_\mathfrak{b}\ \omega$
Bachelor Thesis (2008)

[61] M. J. Galuska:
New Horizons in Particle Physics –
From the Higgs Boson to Dark Matter at the LHC
On the Invited Talk Given by Karl Jakobs, University of Freiburg (2009)

Appendix

A. Assumed Parameters for Simulation of X(3872) Resonance Scan at $\overline{\text{P}}$ANDA

Resonance Scan	
Experiment	$\overline{\text{P}}$ANDA
Resonance	X(3872)
Decay Channel	$J/\psi\ \pi^+\pi^-$
Subsequent Decay	$J/\psi \to \mathrm{e}^+\mathrm{e}^-$
Number of scan points	20
Spacing	Equidistant
E_{cm} interval	$[3871.54\ \mathrm{MeV}, 3872.49\ \mathrm{MeV}]$
HESR	High resolution mode
p_{beam} distribution	Gaussian, rms $\Delta p_{\mathrm{beam}}/p_{\mathrm{beam}} = 2 \cdot 10^{-5}$
E_{cm} distribution	Gaussian, rms from eq. (26)
Accelerator duty factor	50%
Integrated luminosity	0.864 pb^{-1}/day
X(3872)	
Mass $m_{\mathrm{X(3872)}}$	3.872 GeV
Width $\Gamma_{\mathrm{X(3872)}}$	100 keV
Cross section model	Breit-Wigner, eq. (20)
Production cross section in $\mathrm{p\overline{p}}$	$\sigma_{\mathrm{BW}} = 50$ nb for $E_{\mathrm{cm}} = m_{\mathrm{X(3872)}}$
Branching Ratio into $J/\psi\ \pi^+\pi^-$	0.1
Decay model	VVPiPi
Subsequent J/ψ Decay	
Branching Ratio into $\mathrm{e}^+\mathrm{e}^-$	0.06
Decay model	VLL
Background Processes	
Direct: $\mathrm{p\overline{p}} \to J/\psi\ \pi^+\pi^-$	$\sigma = 1.2$ nb for $E_{\mathrm{cm}} \simeq m_{\mathrm{X(3872)}}$
All other	Assumed to be suppressible with PID

Table 4: Summary of the parameters used for the simulation of a resonance scan of X(3872) at $\overline{\text{P}}$ANDA. The entire simulation chain from event generation, over transport, digitization, reconstruction, particle identification and analysis is carried out in the PandaRoot framework.

B. Detector Setup Code Used for Simulation of X(3872) Resonance Scan at $\overline{\mathrm{P}}$ANDA

```
FairModule *Cave= new PndCave("CAVE");
Cave->SetGeometryFileName("pndcave.geo");
fRun->AddModule(Cave);

FairModule *Magnet= new PndMagnet("MAGNET");
Magnet->SetGeometryFileName("FullSuperconductingSolenoid_v831.root");
fRun->AddModule(Magnet);

FairModule *Dipole= new PndMagnet("MAGNET");
Dipole->SetGeometryFileName("dipole.geo");
fRun->AddModule(Dipole);

FairModule *Pipe= new PndPipe("PIPE");
fRun->AddModule(Pipe);

PndTpcDetector *Tpc = new PndTpcDetector("TPC", kTRUE);
Tpc->SetGeometryFileName("tpc.geo");
Tpc->SetAliMC();
fRun->AddModule(Tpc);


FairDetector *Mvd = new PndMvdDetector("MVD", kTRUE);
Mvd->SetGeometryFileName("Mvd-2.1_FullVersion.root");
fRun->AddModule(Mvd);

PndEmc *Emc = new PndEmc("EMC",kTRUE);
Emc->SetGeometryVersion(19);
Emc->SetStorageOfData(kFALSE);
fRun->AddModule(Emc);


PndMdt *Muo = new PndMdt("MDT",kTRUE);
Muo->SetBarrel("fast");
Muo->SetEndcap("fast");
Muo->SetMuonFilter("fast");
Muo->SetMdtMagnet(kTRUE);
Muo->SetMdtMFIron(kTRUE);
fRun->AddModule(Muo);

FairDetector *Gem = new PndGemDetector("GEM", kTRUE);
Gem->SetGeometryFileName("gem_3Stations.root");
fRun->AddModule(Gem);

PndDsk* Dsk = new PndDsk("DSK", kTRUE);
Dsk->SetGeometryFileName("dsk.root");
Dsk->SetStoreCerenkovs(kFALSE);
Dsk->SetStoreTrackPoints(kFALSE);
fRun->AddModule(Dsk);

PndDrc *Drc = new PndDrc("DIRC", kTRUE);
Drc->SetRunCherenkov(kFALSE); // for fast sim Cherenkov -> kFALSE
fRun->AddModule(Drc);
```

Note that for the other results presented in this thesis the detector setup used slightly different geometry versions of the subdetectors.

C. Documentation of Developed Software

The software developed in this work consits of several PandaRoot macros and scripts written for the popular Unix shell *bash* (Bourne-again shell) which is available for every major operating system. The same holds for PandaRoot with the exception of Microsoft Windows. The software collection will be made available to the $\overline{\text{P}}$ANDA collaboration and has already been used successfully for related work [48].

For the following procedure it is assumed that a computer with a working PandaRoot installation is used. Furthermore, the open source software Torque Maui (or any compatible batch farm software) is required to be installed.

There are generally three distinct scenarios for the use of the software package developed for this thesis:

Repeat a resonance scan simulation: For instance after major updates of the PandaRoot framework or the $\overline{\text{P}}$ANDA detector setup a user might want to check whether the results obtained with previous versions have changed significantly. All the user has to do is to set the PandaRoot environment for the desired revision, navigate to the folder that contains the scripts and root macros and then just call the central control script *batch.sh*. It takes care of the splitting of the total simulation project into small parts which are automatically submitted as jobs to the batch farm. Then the job is processed on a computing node, i.e. the server assigned by the so-called headnode of the batch farm for processing the job . The data handling for the most efficient use of the resources and to comply with the cluster guidelines outlined in [44] is automatically accounted for by a subscript called *sim.sh*. The user simply has to wait until the final results are ready and can check the progress by calling a script called *progresscheck.sh* from the folder that will contain the results. *progresscheck.sh* can automatically detect jobs that did not finish successfully, for instance due to hardware failures. Those can automatically be deleted and resubmitted to the batch farm by the script. Once the data is processed, the plots will be automatically created in a subfolder called *plots*.

Major software changes might require to adapt the utilized PandaRoot macros, but the scripts should not need to be touched.

Add a resonance scan for another particle R: This requires to adjust the parameters of the central shell script *batch.sh* and the analysis PandaRoot macro *run_ana_tpcorsttcombi.C*. Mass, width and cross section for $\text{p}\overline{\text{p}} \to R \to f$ can be adjusted in the script. The analysis macro needs to be adjusted for the final state of interest f.

Add more features: This will require a more detailed knowledge of the individual shell scripts and PandaRoot macros. Different additional features need to be implemented in different places. Therefore, a brief explanation of the basic concepts of each script and macro is given. More details can be found in the elaborate comments contained in the software.

batch.sh: As the name indicates, this script is used to submit jobs to the batch farm. It contains all important simulation parameters and is used as a convenient interface for the user who can choose between predefined types of simulations to be carried out. *batch.sh* is not much more than a straightforward implementation of a *for loop* which copies the original source folder to the folder that is supposed to store the simulation results and then it calls a set of two scripts which submit a call of the script *sim.sh* to the batch farm. *sim.sh* controls the actual chain of PandaRoot macros which perform the simulations. *batch.sh* exports its arguments as envrionment variables for *sim.sh* which passes them on to the PandaRoot macros.

sim.sh: Is usually called via *batch.sh* and then executed on the batch farm. However, it also features an interactive mode which can conveniently used for debugging or when no batch farm software is available. When called via *batch.sh* it takes care of the data handling from the headnode of the batch farm to a temporary folder on the executing host's harddisk. It checks whether there are

problems such as "insufficient user rights for the directory" or "disk full" and stops the execution if there is an error condition. Otherwise, it calls the five PandaRoot simulation macros and protocols their output into log files. Once a job finishes successfully, the data is moved back onto the headnode. If individual PandaRoot macros fail, it tries three times to re-execute the according macro. This should usually fix randomly occuring root crashes which happen in less than 1% of all simulations.

PandaRoot macros: The simulations are carried out by four PandaRoot macros which are adjusted versions of the well-known preexisting macros. Most notably they were unified for Geant3 and Geant4 and the TPC and STT detector layout. By passing a random seed which is derived from a variable exported by *batch.sh*, the macros can be used to parallelize the workload. *run_sim_tpcorsttcombi.C* can use events created externally with DPM or EvtGen or can call either of those generators directly for live event generation. When called in "resonance scan mode", it calculates how many events need to be simulated for the current resonance scan point. Otherwise, *sim.sh* passes the number of events to simulate. Either Geant3 or Geant4 can be used to transport the particles from the generated events through the $\overline{\text{P}}$ANDA detector. Interaction with the detector materials and particle decays are simulated.

run_digi_tpcorsttcombi.C is used for digitization. In this step of the simulation the signals of the individual detectors and their processing in the front-end-electronics are modeled based on the results from the transport of particles through the detector. The idea is to make the simulated data as similar as possible to real data so that it can be processed and analysed using the same software as real data.

run_reco_tpcorsttcombi.C and *run_pid_tpcorsttcombi.C* are used to reconstruct and identify charged and neutral particles based on the digitization results.

run_ana_tpcorsttcombi.C is not called by sim.sh for technical reasons. This script corresponds to a user's analysis macro in which the reconstructed and identified particles can be used to reconstruct the final state of interest.

progresscheck.sh: The user can check the progress of the simulation by calling this script which is automatically copied to the result directory by *batch.sh*. The script also scans the log files and can automatically delete jobs which were not finished successfully. These jobs can be resubmitted to the batch farm if the user wishes to do so.

D. The Computing Cluster

In early 2010 our work group acquired a new cluster. Since then it has been used for simulation and data analysis mostly for the PANDA, BES and Belle experiments. From the careful selection and the physical installation of the hardware to the software installation and configuration, all steps were carried out by members of our work group.

The total computing power of the cluster amounts to 18 Intel Xeon E5520 Quad-Core CPUs that can run a total of 144 threads in parallel with 108 GB of DDR3 ECC RAM, distributed over 9 servers, all connected by multiple 1 GBit ethernet lanes. The cluster's main storage is provided by an external RAID system that has been equipped with 24 consumer grade hard disks of 2 TB capacity in a RAID 5 array with one hot spare amounting to a net capacity of 44 TB. The home directories are located on a set of two mirrored 1 TB server grade hard disks. Eight 250 GB server grade drives are used in the computing servers for the operating systems and for temporary storage of intermediate results.

All cluster servers run *Scientific Linux CERN (SLC) 5.5 x86_64*. A combination of *Torque* and *Maui* (see section 2) is used to distribute jobs on all servers and to use the available computing power in the most efficient way. The user home directories are backed up on tape on a daily basis. The cluster's state can be monitored live over the internet with the installed Ganglia monitoring system. A screenshot is shown in figure 17. Further details can be found in [44].

Figure 17: A view on the cluster's load with Ganglia during the simulation of 10^7 inelastic $p\overline{p}$ background events for the resonance scan of the X(3872) performed in this work. See also section 6.3.

Acknowledgements

First and foremost, I would like to thank Prof. Dr. Wolfgang Kühn for incorporating me into his work group and enabling me to write this thesis. I have appreciated his scientific advice and guidance at key moments in my work. The employment as one of the work group's server administrators as well as a tutor for his lectures have allowed me to gather valuable experience which motivated me to do my best again and again. I appreciate his support for an application to the Studienstiftung des deutschen Volkes (National Academic Foundation).

In the same way, I would like to use this opportunity to express my gratitude to Prof. Dr. Alfred Müller whose letter of endorsement gave me the chance to apply for the aforementioned stipend of which I have benefited in many respects.

In the same regard, I would like to thank Prof. Dr. Ulrich Mosel, Prof. Dr. Horst Lenske and the people working for the German Academic Exchange Service for having supported me during my stay abroad to study at the University of Washington in Seattle for almost one year.

I thank AR Dr. Jens Sören Lange most sincerely for supervising my thesis, for his scientific and stylistic advice, for the careful reading of numerous drafts of this thesis and for many suggestions on how to improve it. I am very impressed with him both from an academic point of view as well as from a personal point of view. He was always amenable when questions arose which he answered very friendly and with great patience even though he must have been extremely busy supervising many complementary projects at the same time. He was both very understanding and supportive when I had to spend my attention to other fields of study which allowed me to benefit greatly both in scientific and personal ways. I would like to exemplarily mention the probability theory lecture given by Prof. Dr. Häusler which helped me considerably in understanding the mathematical foundations of this work.

I would like to thank Dr. Björn Spruck for giving advice and helpful suggestions on many physics and especially software related occasions. Especially, his deep understanding and knowledge of Linux, root and PandaRoot made him always a helpful link between a given problem and its solution. Many times he pointed me into the right direction which saved me a lot of possibly unnecessary work. The more so as the software interface to the batch farm used by the scripts and macros developed in this work is based on scripts originally written by him. In addition, he played a key role in finding possibly weak links in the structure of this master thesis.

My thanks for answering numerous PandaRoot related questions and supplying the basis for most of the root macros which were developed and used in this thesis go to Dr. Stefano Spataro.

I thank Dr. Yutie Liang for helpful conversations and reading recommendations which improved my understanding of detailed balance.

Furthermore, I thank Stephanie Künze for the pleasant work climate in the mutually used office, for her support and encouragement, especially to the end of this work. Thomas Geßler, Andreas Kopp and Sören Fleischer were always proficient conversational partners – especially in the beginning of the thesis – when many questions about Linux arose. They were also a great help every time a problem with our workgroup's cluster needed to be solved. I would like to thank Ingo Heller for recreating and inspiring lunch time conversations and Svende Braun, David Münchow, Diego Semmler, Matthias Ullrich, Milan Wagner and Marcel Werner for their friendly support.

I would like to acknowledge and thank for useful conversations with Dr. Thomas Würschig, Dr. Marius Mertens, Tsitohaina Randriamalala and Tobias Weber from the $\overline{\text{PANDA}}$ collaboration.

Last, but not least, I thank my family, relatives and friends for their understanding and their support.

I wish Stephanie Künze and Ingo Heller – who both left the work group during the finalisation phase of this thesis – all the best for their future careers and personal lifes.

This work was supported in part by BMBF (06GI9107I) and the LOEWE-Zentrum HICforFAIR.

Ich versichere, dass ich diese Masterarbeit selbständig geschrieben und deren Inhalt wissenschaftlich erarbeitet habe. Außer der angegebenen Literatur und Software habe ich keine weiteren Hilfsmittel verwendet.

Pohlheim, den 31.05.2011 Martin Johannes Galuska